REPORT 109

ADVISORY GROUP FOR AERONAUTICAL
RESEARCH AND DEVELOPMENT

REPORT 109

FLIGHT LOADS MEASUREMENTS ON NACA RESEARCH AIRPLANES

by

De E. BEELER

APRIL—MAY 1957

NORTH ATLANTIC TREATY ORGANIZATION
PALAIS DE CHAILLOT, PARIS 16

REPORT 109

NORTH ATLANTIC TREATY ORGANIZATION

ADVISORY GROUP FOR AERONAUTICAL RESEARCH AND DEVELOPMENT

FLIGHT LOADS MEASUREMENTS ON NACA RESEARCH AIRPLANES

by

De E. Beeler

This Report was presented at the Fifth Meeting of the Structures and Materials Panel, held from 29th April to 3rd May, 1957, in Copenhagen, Denmark

SUMMARY

Flight loads investigations are conducted primarily for the purpose of confirming wind-tunnel results by comparing the full-scale results with comparable wind-tunnel results as frequently as deemed necessary; assessing the maneuvering conditions required of the aircraft and determining the associated dynamic loading conditions for the maneuvers; and bringing to light loads problems as a result of conducting flight research. The research airplane program in the United States included from the beginning extensive programs on flight loads measurements. This Report summarizes some of the results from these investigations for three aircraft: the X-1 rocket-powered airplane; the X-5 variable-sweep airplane; and the XF-92A delta-wing airplane.

SOMMAIRE

Les mesures relatives aux charges de vol s'effectuent en premier lieu dans les buts suivants: vérification des résultats d'essais en soufflerie en comparant, aussi souvent que l'on juge nécessaire, les résultats obtenus avec l'avion en vraie grandeur et les résultats comparables obtenus à partir d'essais en soufflerie; évaluation des conditions de manoeuvrabilité demandées à l'avion et détermination des conditions de charge dynamique correspondant aux différentes manoeuvres; mise en lumière, par suite des recherches effectuées en vol, de problèmes concernant les charges. Le programme d'essais établi pour les avions de recherche aux Etats-Unis a prévu, dès le début, des travaux poussés sur les mesures de charges de vol. Cette communication donne en résumé certains des résultats d'études réalisées sur trois avions: l'avion X-1 à fusées, l'avion X-5 à flèche variable et l'avion XF-192A à aile en delta.

629.13.012:629.135.072.2

3c6d2c

CONTENTS

LIST OF FIGURES

NOTATION

b_v	vertical-tail panel span, ft
$b_w/2$	wing-panel semispan, ft
C_{b_v}	bending-moment coefficient of vertical tail, $M_v/qS_v b_v$
C_{b_w}	bending-moment coefficient of wing panel, $M_w/qS_w b_w/2$
$(C_{m_o})_{wf}$	pitching-moment coefficient of wing-fuselage at zero lift, $M_o/qS\bar{c}$
C_N	normal-force coefficient based on total wing area, N/qS
C_{N_A}	airplane normal-force coefficient, nW/qS
C_{N_t}	horizontal-tail normal-force coefficient, L_t/qS_t
C_{N_w}	wing-panel normal-force coefficient, L_w/qS_w
$\frac{dC_{N_w}}{dC_{N_{wf}}}$	fraction of total wing-fuselage load carried by a wing
C_{Y_v}	vertical-tail panel side-force coefficient, L_v/qS_v
c_{av}	average wing-panel chord, ft
c_n	section normal-force coefficient
$c_n(c/c_{av})$	section normal-load parameter
$\bar{c}$	wing mean aerodynamic chord, M.A.C., ft
$\bar{c}_w$	wing-panel mean aerodynamic chord, ft
h_p	pressure altitude, ft
L_t	aerodynamic horizontal-tail load, positive for up load, lb
L_v	aerodynamic load on vertical-tail panel, lb
L_w	aerodynamic load on wing panel, lb
M	Mach number
M_v	vertical-tail panel aerodynamic bending moment about strain-gage station, ft lb
M_w	wing-panel aerodynamic bending moment about strain-gage station, ft lb

M_o	pitching moment at zero lift, ft lb
N	normal force of airplane, lb
n	normal acceleration, g units
Δ_n	incremental normal acceleration, g units
P	pressure coefficient, $(p - p_o)/q$
P_R	resultant pressure coefficient, $P_l - P_u$
p	local static pressure, lb/sq ft
p_o	free-stream static pressure, lb/sq ft
p_{max}	maximum rolling angular velocity, radians/sec
q	dynamic pressure, $1/2\rho V^2$, lb/sq ft
$\dot{q}$	pitching angular acceleration, radians/sec^2
S	wing area, sq ft
S_t	horizontal-tail area, sq ft
S_v	vertical-tail area, sq ft
S_w	area of one wing panel, sq ft
V	true airspeed, ft/sec
W	airplane weight, lb
$(x_{ac})_{wf}$	wing-fuselage aerodynamic center, % M.A.C.
x_{cp}	chordwise center of pressure, % $\bar{c}_w$
y_{cp}	lateral center of pressure, % $b_w/2$
α	airplane angle of attack, deg
β	airplane angle of sideslip, deg
Λ	angle of sweep, deg
ρ	density of air, slugs/cu ft

Subscripts

l	lower	u	upper	max	maximum

FLIGHT LOADS MEASUREMENTS ON NACA RESEARCH AIRPLANES

De E. Beeler*

1. INTRODUCTION

Flight loads investigations are conducted primarily for the purpose of confirming wind-tunnel results by comparing the full-scale results with comparable wind-tunnel results as frequently as deemed necessary; assessing the maneuvering conditions required of the aircraft and determining the associated dynamic loading conditions for the maneuvers; and bringing to light loads problems as a result of conducting flight research. It was natural, therefore, from the beginning of the research airplane program in the United States, to include extensive programs on flight loads measurements. This presentation is intended to summarize some of the results from these investigations.

Generally, the data have been selected from three research aircraft having a wide range of configuration. The aircraft selected are shown in Figure 1. Included are the X-1 rocket-powered airplane which has a straight wing with a thickness ratio of 10% of the chord and a moderately high horizontal tail; the X-5, a variable-wing-sweep airplane with a wing airfoil section thickness of about 6% of the chord at 60° of sweep and the horizontal tail near the center line of the extended wing chord; the XF-92A delta-wing aircraft having a wing thickness of about 6.5% of the chord and having no horizontal tail. The measured loads data presented for the X-5 will be for the 60° wing sweep configuration. The flight loads for the various components of these aircraft were determined by use of calibrated strain gages. In addition, pressure-distribution measurements were also made of the fuselage and the wing of the X-1 airplane.

2. FLIGHT ENVELOPE FOR RESEARCH AIRCRAFT

In the flight investigation of the research aircraft, it has been found that maximum lift coefficient of the airplane or the design load factor does not necessarily establish the boundaries for the operating flight envelopes of the aircraft. The occurrence of pitch and yaw divergences and inertia coupling have caused the aircraft to reach or exceed design limits inadvertently, and the occurrence of buffeting, changes in longitudinal stability, loss in control power, and high induced drag have prevented the attainment of maximum lift. A typical flight envelope of a research aircraft is shown in Figure 2, where the angle of attack for maximum lift coefficient is plotted against Mach number. The usual reduction in maximum lift at transonic speeds is evident with increases in maximum lift at supersonic speeds. Also included as a lower boundary defining an abrupt change in longitudinal stability (referred to as 'pitch-up') and also defining the increase in buffeting intensity. The shaded area between the two boundaries becomes

---

* *Chief, Research Division, NACA High-Speed Flight Station, Edwards Air Force Base, California, U.S.A.*

an area of questionable use for normal flying of aircraft. The extent of the shaded area will depend on the aircraft configuration, but, generally speaking, the use of thin airfoil sections will reduce the occurrence of transonic buffet to an area near maximum lift. The improper use of aircraft arrangements such as wing sweep, aspect ratio, and horizontal-tail position will result in an area below maximum lift of questionable usage. Flight loads investigations conducted in the shaded areas have shown nonlinearities in the various loading parameters, as will be pointed out.

3. DIVISION OF TOTAL AIRPLANE LOAD

The loads on the wing and tail panels were measured independently of the total airplane load; therefore, it was possible to determine the division of the normal load between the wing, tail, and fuselage. Typical data for the straight-wing X-1, swept-wing X-5, and the delta-wing XF-92A are shown in Figure 3 for a subsonic and transonic Mach number, and are shown as component normal-force coefficients plotted against the airplane normal-force coefficient. The airplane load was determined from the measurement of the normal accelerations at the airplane center of gravity and a knowledge of the weight of the airplane. The wing loads for the X-1 were obtained from pressure-distribution measurements and calibrated strain gages and the remaining wing and tail loads were obtained from calibrated strain gages. The fuselage loads were determined indirectly by subtracting the sum of the wing and tail loads from the total airplane load. All loads are presented as aerodynamic loads. As may be noted from the figure, the straight-wing aircraft showed linear variations throughout the normal-force-coefficient range investigated. The highly swept and delta-wing aircraft show reductions in wing load at the higher values of airplane normal force and corresponding increases in fuselage loads. Slopes of the wing and fuselage data in the linear range have been evaluated to determine the contribution of the wing load to the wing-fuselage load and are shown in Figure 4 as a function of Mach number. The measured results show only slight increases in wing-load contribution with Mach number. Calculations of the wing-load contribution to the wing-fuselage load were made for the configuration shown by using the methods of Hopkins and Carel[4]. The method was developed from the use of wind-tunnel results and the use of theoretical results from Multhopp, DeYoung, Weissinger, and Lennertz and include the interference effects of the fuselage on the wing and of the wing on the fuselage. A comparison of the calculations with the flight data shows that a reasonably good prediction can be made of the division of normal-force loads between the wing and the fuselage at the subsonic speeds.

4. CHORDWISE PRESSURE DISTRIBUTION

The chordwise pressure distributions of the upper and lower surfaces of a mid-semispan station of the 10% thick X-1 wing for subsonic, transonic, and supersonic speeds are shown in Figure 5 and illustrate the general shape and change in shape of the pressure diagrams for these speed regimes (see also Reference 2). The subsonic distribution is of the triangular shape with peak pressures occurring at the airfoil leading edge with the center of pressure forward on the airfoil section. The distribution at transonic speed is irregular as a result of normal shock formations on the upper and lower surfaces. For the particular flight condition presented in Figure 5, the normal shock, as defined by the abrupt pressure recovery

between 40 and 50% of the chord, is located on the upper surface at approximately 40% of the chord. Separated flow region exists to the rear of the 50% chord as indicated by the flat negative pressure portion of the pressure diagram. The normal shock on the lower surface is located near the 80%-chord position. As a result of the existence of normal shock formations in the transonic region, variations in angle of attack and Mach number have been found to vary greatly the detail pressure distribution at transonic speeds. Flight results from thinner airfoil sections indicate that the large irregularities in the distributions are greatly reduced by use of the thinner airfoil sections. At the supersonic speeds, the largest change from the subsonic distribution has been in the upper surface distribution of load where at supersonic speeds the largest negative pressure now exists over the rearward portion of the wing section.

5. SPANWISE DISTRIBUTION OF SECTION CHORDWISE LOADING

Section load distribution across the span of the X-1 wing[3,4] is shown in Figure 6 for subsonic, transonic, and supersonic Mach numbers at a nominal wing-panel normal-force coefficient. As may be noted, there is the gradual change from a triangular type of loading with the center of load forward on the section at subsonic speeds to an approximate rectangular loading with the center of pressure located at approximately the midchord station. The irregular shape of the distribution is apparent at the transonic speeds. No pertinent chordwise load-distribution changes, from the loads standpoint, appear to exist for the section loading across the span. Calculations of the chordwise loading have been made to illustrate the degree of correlation that might be expected where compared with full-scale flight results. The results of the calculations are shown in Figure 6. The geometry of the exposed panel was used and a reflection plane at the fuselage junction assumed. For the data of a Mach number of 0.53, chordwise load distributions were determined by application of a similar analysis as given in Reference 5. The section load at each span station was adjusted to a span load distribution calculated by the method of Reference 6 and corrected by the Prandtl-Glauert factor for compressibility effects. As may be seen, very good agreement is obtained with the experimental data for all span stations. The measured data at a Mach number of 0.88 show, as might be expected, a strong evidence of mixed flow conditions over the wing surface. Calculations for the prediction of the local pressure loading over the airfoil are surely subject to question; however, results of the calculations are shown to give some qualitative idea of the comparison between theory and experiment at this Mach number. In the calculations, (a) the Prandtl-Glauert transformation was used to correct the span loading for compressibility effects, (b) the flat-plate pressure distributions at angle of attack were calculated by an application of the results of Guderley[7], (c) the pressure distribution due to thickness was calculated by an application of the results of Spreiter and Alksne[8].

The calculations for the supersonic case used the panel as a flat plate and applied the linearized theory results of Reference 9 which consider only airfoils at supersonic Mach numbers in which both the leading and trailing edges are supersonic. Additional calculations for the same station are shown projected to the right of Figure 6 where the upper and lower surface pressure distributions were calculated by an application of Busemann's second-order theory[10] assuming that (a) the mid-semispan wing station is in a two-dimensional flow region (the root

and tip linearized shock lines intersect in the neighborhood of the trailing edge), and (b) the airfoil of this span location was approximated by a biconvex profile. The comparison between the calculations and measured data shows good agreement. The use of the expansion theory of Reference 10 improved the prediction somewhat over the linearized theory. Similar section loading data of Figure 6 are shown in Figure 7 to illustrate the distribution of loading for high angles of attack. The data of Figure 7 are for angles of attack near the maximum lift of the wing. The increase of the rear chord loading at the higher Mach numbers is evident, as for the low angles of attack. Also, the existence of high pressure loads at the leading edge of the wing for all Mach numbers may be noted.

6. SPANWISE LOAD DISTRIBUTION

An integration of the section load distribution over the span of the wing gives the span loading distribution shown in Figure 8. The data are extended to include the pressure distribution measured over the fuselage to the airplane center line. It may be noted that an appreciable reduction in load over the fuselage exists and an eliptical loading is shown for the subsonic and supersonic Mach numbers. Irregularities do exist, however, in the span loading at all transonic speeds similar to that shown in Figure 8 at a Mach number of 0.88. An inspection of the detailed surface pressure distribution shows that irregular chordwise normal shock location and movement at various span stations produce the irregular effect in the span loading. Calculations were performed by the methods outlined and discussed previously with Figure 6. Good agreement was realized by the span load distributions at subsonic and supersonic speeds. The irregularities in the experimental data were of course not predicted.

7. COMPARISON OF FLIGHT AND WIND TUNNEL SECTION LOADINGS

It is desirable, when deemed necessary, to compare the results from full-scale flight investigations with comparable results from wind-tunnel investigations. The degree of correlation found in these comparisons is illustrated in Figure 9. The data are results from investigations, conducted in the NACA Langley 16 ft transonic tunnel, of a model of the X-1 airplane[11] and the flight results. It may be noted that there are some differences in the detailed loading; however, it is felt that the agreement is fairly good. It should be pointed out that the airplane trailing edges were cusped and the airplane sections were modified toward uncusping that area. This would account for some of the differences at the trailing edges. The comparison of span loading results from flight and wind-tunnel tests is presented in Figure 10. The normal-load distributions show good agreement between the wind tunnel and flight. On the basis of comparisons similar to those made, it is believed that good correlation can be expected from wind-tunnel and flight investigations of steady-state loads.

8. EFFECT OF MACH NUMBER ON WING LATERAL CENTER OF PRESSURE

The effect of Mach number on the lateral center of pressure of the wing panel from an integration of wing span load distribution is shown in Figure 11 for the

X-1 wing. Included also are similar data for the swept-wing X-5 and delta-wing XF-92A. The data are for regions where linear variations of wing load with angle of attack existed. For the straight- and swept-wing configurations, no change in lateral center of pressure with Mach number is evident. For the delta-wing configuration, there was a gradual outboard movement in center of pressure with Mach number. Results of calculations by the methods of Reference 6, which do not include the effects of the fuselage, are also included. The calculations for the straight- and delta-wing airplanes show good agreement with the flight data. However, the calculations for the swept-wing airplane show a location further inboard than the flight data. Additional calculations for the X-5 airplane, including the effects of the fuselage[12], were made and showed only a negligible effect.

The wing bending-moment coefficients for the three configurations are shown in Figure 12 as a function of wing-panel normal-force coefficient. For the X-1 airplane, the bending-moment load varies linearly with wing load, indicating a constant lateral center of pressure with increasing airplane lift. However, for the swept-wing and delta-wing aircraft appreciable reductions in bending moment are evident at the higher wing-panel normal-force coefficients.

9. EFFECT OF MACH NUMBER ON WING CHORDWISE COEFFICIENT

The variation of the wing chordwise center of pressure with Mach number is shown in Figure 13 for the three airplane configurations. For the straight thick airfoil, considerable variation in center of pressure is evident at the transonic speeds. It would be expected, however, that for thinner airfoil sections these magnitudes would be reduced, becoming only a gradual transition from the subsonic to the supersonic speeds. These trends are indicated to some extent with the thinner swept sections of the X-5 and XF-92A airplanes shown in the lower portion of the figure.

10. FUSELAGE PRESSURE DISTRIBUTION

Typical results of the fuselage pressure distribution of the X-1 airplane are shown in Figure 14 for Mach numbers of 0.80 and 1.00 (Ref.13). Also included are typical pressure distributions for the wing. The extent to which the pressure distribution of the wing carries over and influences the local pressures of the fuselage in the vicinity of the wing may be noted. Immediately forward of the wing station a reduction in negative pressure in the fuselage distribution results due to the wing compression followed by an approximate image of the wing distribution on the fuselage body.

11. VARIATION OF TAIL LOAD WITH AIRPLANE LOAD

The measured horizontal-tail load with airplane normal-force coefficient for the X-1 airplane is shown in Figure 15 (Ref.14). The variations in tail load with normal-force coefficient are linear for the lift ranges shown, but vary considerably depending on the speed range due to changes in the aerodynamic center of the wing-fuselage combination as shown in Figure 16. The data of Figure 16 were computed from measured tail loads and show that the aerodynamic center of the wing-fuselage

combination moves abruptly from a subsonic level at transonic speeds to a rearward position at supersonic speeds. Also shown in the figure is the effect of Mach number on the zero pitching moment of the wing-fuselage combination as calculated from the measured flight tail loads. It is possible, therefore, by using these flight data or similar data from wind-tunnel tests and by assigning proper flight pitching accelerations, to calculate the horizontal-tail loads for symmetrical maneuvering flight. Figure 17 shows the variation of the measured tail loads at subsonic, transonic, and supersonic Mach numbers for the swept-wing X-5 airplane[15]. It may be noted that nonlinearities exist throughout the lift region both for subsonic and for transonic speeds. It would be necessary in these cases to make detailed measurements of the tail loads in wind-tunnel tests to obtain basic data if accurate prediction of the flight tail loads is required.

12. EFFECT OF WING SWEEP ON GUST RESPONSE

The unique feature of being able to change the wing sweep angle of the X-5 afforded the opportunity of investigating the effects of sweep on the gust response of the airplane flying in turbulent air. The aircraft was flown over a prescribed air course at a given indicated airspeed in turbulent air with sweep angles of 20°, 45°, and 59°. The measured results are shown in Figure 18 as the ratio of the loads of a swept-wing airplane for the three wing sweep angles. Included also is the load ratio as a function of the cosine of the angle of sweep. The flight data at the two lower sweep angles agree with the cosine concept; however, the load-ratio data at a wing sweep angle of 59° are slightly higher. Due to the low lateral damping of the airplane at the high wing sweep angles some rolling was evidenced in the measured data. It is believed that some of the differences noted at the high sweep angles may result from the normal acceleration due to the rolling.

13. EFFECT OF AIRFOIL THICKNESS ON BUFFETING

The occurrence of buffeting at transonic speeds was most objectionable with the early research aircraft. The regions of most concern are illustrated in Figure 19 where boundaries of the buffet region are shown for the straight-wing X-1 airplane. Measured maximum fluctuating stresses in the primary structure of the wing and tail were of the order of 15 to 20% of the design stresses. The use of thin airfoil sections has essentially eliminated the transonic buffet region, as shown by the boundary for a thin airfoil. However, at subsonic speed buffeting occurs at low angles of attack and devices such as leading-edge flaps are found to be beneficial for raising the boundary level, as shown in the figure.

14. UNCONTROLLED MANEUVERS

Maneuvers of an uncontrolled nature have been encountered during the flight investigations of the research aircraft that are of interest to the study of flight loads. These maneuvers have manifested themselves in the form of divergences in pitch and in yaw during flight at high angles of attack and during rolling maneuvers. Typical examples of the development of angles of yaw and angles of attack during

the maneuvers are shown in Figure 20. Also included are the pitching accelerations experienced during the inadvertent maneuvers. The open and solid symbols define the maximum measured values resulting from inadvertent pitching maneuvers and rolling maneuvers, respectively.

For the pitch-up maneuvers it may be noted that the pitching acceleration experienced during recovery was approximately twice the values experienced during the inadvertent pitch-up. The horizontal-tail and wing loads measured during the maneuvers were below design limits since they were performed at high altitude; however, extrapolation to higher dynamic pressures shows that design loads may easily be exceeded.

15. EFFECT OF YAW ON VERTICAL-TAIL LOADS

The loss in directional stability at high Mach number and at high angles of attack has resulted in development of large yaw angles. The magnitude of angles for high angle-of-attack conditions is shown in Figure 20. It is of interest to review the measured vertical-tail loads experienced during these yawing maneuvers which occurred at an angle of attack of approximately 20°. Figure 21 shows the variation of the measured vertical-tail load with sideslip angle and the vertical-tail load with vertical-tail-bending moment. These data show appreciable losses in vertical-tail load and change in vertical-tail-load distribution with increasing yaw angles. The loss in tail load, of course, reduces the tail contribution to static directional stability, hence the development of high sideslip angles. These high angles of yaw not only produce high vertical-tail loads but also subject the fuselage body to high loads. The changes in load distribution of the vertical tail are apparent from the appreciable outboard movement in the lateral center of pressure. Studies of the flow behavior at the tail plane of an X-5 model in the NACA Langley stability tunnel have been made at low speed by using the tufted screen grid technique. These studies have shown vortices to originate from the wing at high angles of attack as illustrated in Figure 22. The illustration shows the model at an elevated angle of attack and in a yawed attitude. In the lower portion of the figure is illustrated the location of the vortices in relation to the vertical-tail plane of the X-5. These were determined from inspection of the tuft screen photographs at an angle of attack of 22° for three conditions of yaw. The figure also illustrates the effect of the vortice on the vertical-tail loading as the vortice approaches the tail surface in a yawed condition. The local angles of attack of the tail surface are increased due to the presence of the vortex above the plane of the vortex center and are decreased below the vortex center. For the location of the horizontal tail of the X-5 at these angles-of-attack conditions no appreciable effects of the vortex on the horizontal-tail loading were evident. It would be expected, however, that if the vortices were located near the horizontal-tail plane the distribution of horizontal tail would be affected.

16. VERTICAL-TAIL LOADS DURING ROLLING

Another problem concerned with loads on the research airplane has been the development of large angles of attack and angles of sideslip (Fig.23) during rolling maneuvers. This has occurred on aircraft having the mass distributed primarily along

the fuselage and having the ability to roll at rates approaching the natural circular frequency in pitch or yaw. Measured loads for these conditions at high altitude have approached and in some cases exceeded the design limit during the maneuver. Attempts to alleviate the difficulties have been made by increasing the static directional stability or restricting the rate of roll, or both. These flight experiences have, however, emphasized the need in structural design for a careful and complete study of the stability characteristics of the airplane. It is also necessary to perform calculations of time histories of rolling maneuvers using five-degrees-of-freedom. The use of calculated data has been found helpful in exploring suspected problems of this nature. For instance, the effect of high dynamic pressure for these types of maneuvers may be assessed by typical calculations as shown in Figure 23. These calculations are from an analog study to determine the vertical-tail load during a rolling maneuver and are based on flight results of a rolling maneuver at high altitude. The calculations show appreciable reduction in vertical-tail load for the lower rolling velocities; however, initiating the roll at a higher angle of attack, as in a rolling pull-out, would result in appreciable increases in vertical-tail load at the high dynamic pressures.

17. CONCLUSION

In conclusion, it may be said that the flight loads investigations of the research aircraft have provided considerable full-scale flight loads data which may be used to compare and check results from scale-model tests in wind tunnels; have defined areas for expanding research or conducting in more detail present investigations both in flight and in the wind tunnel; have provided full-scale data under actual flight conditions for use in checking theoretical methods of prediction; and, lastly, have provided data on the structural and aerodynamic loads associated with the evaluation of devices and configurations for improving aircraft in the fields of stability and performance as well as aircraft loads.

REFERENCES

1. Hopkins, Edward J. Carel, Hubert C. *Experimental and Theoretical Study of the Effects of Body Size on the Aerodynamic Characteristics of an Aspect Ratio 3.0 Wing-Body Combination.* NACA RM A51G24, 1951.

2. Beeler, De E. et al. *Measurements of the Chordwise Pressure Distributions Over the Wing of the X-S1 Research Airplane in Flight.* NACA RM L8G21, 1948.

3. Knapp, Ronald J. *Tabulated Pressure Coefficients and Aerodynamic Characteristics Measured on the Wing of the Bell X-1 Airplane in an Unaccelerated Low-Speed Stall, In Push-Overs at Mach Numbers of 0.83 and 0.99, and in a Pull-Up at a Mach Number of 1.16.* NACA RM L51F25, 1951.

4. Knapp, Ronald J. Wilken, Gertrude V. *Tabulated Pressure Coefficients and Aerodynamic Characteristics Measured on the Wing of the Bell X-1 Airplane in Pull-Ups at Mach Numbers from 0.53 to 0.99.* NACA RM L50H28, 1950.

5. Küchemann, D. *A Simple Method for Calculating the Span and Chordwise Loading on Straight and Swept Wings of Any Given Aspect Ratio at Subsonic Speeds.* R. & M. No. 2935, British A.R.C., 1956.

6. DeYoung, John. Harper, Charles W. *Theoretical Symmetric Span Loading at Subsonic Speeds for Wings Having Arbitrary Plan Form.* NACA Rep. 921, 1948.

7. Guderley, Gottfreid. *The Flow Over a Flat Plate with a Small Angle of Attack at Mach Number 1.* Jour. Aero. Sci., Vol. 21, No. 4, April 1954, pp. 261-274.

8. Spreiter, John R. Alksne, Alberta. *Theoretical Prediction of Pressure Distributions on Nonlifting Airfoils at High Subsonic Speeds.* NACA Rep. 1217, 1955. (Supersedes NACA TN 3096).

9. Martin, John C. et al. *Calculation of Lift and Pitching Moments Due to Angle of Attack and Steady Pitching Velocity at Supersonic Speeds for Thin Sweptback Tapered Wings With Streamwise Tips and Supersonic Leading and Trailing Edges.* NACA TN 2699, 1952.

10. Busemann, Adolf. *Aerodynamic Lift at Supersonic Speeds.* Luftfahrtforschung, Vol. 12, 1935, pp. 210-220. (Paper Read at 5th Volta Congress, Rome, Italy, Sept. 30 to Oct. 6, 1935).

11. Runckel, Jack F.
Henderson, James H.

A Correlation With Flight Tests of Results Obtained From the Measurement of Wing Pressure Distributions on a 1/4-Scale Model of the X-1 Airplane (10% Thick Wing). NACA RM L52E29, 1952.

12. Zlotnick, Martin.
Diederich, Franklin W.

Theoretical Calculation of the Effect of the Fuselage on the Spanwise Lift Distribution on a Wing. NACA RM L51J19, 1952.

13. Knapp, Ronald J.
et al.

Fuselage Pressures Measured on the Bell X-1 Research Airplane in Transonic Flight. NACA RM L53I15, 1953.

14. Rogers, John T.

Horizontal-Tail Load Measurements at Transonic Speeds of the Bell X-1 Research Airplane. NACA RM L53F30, 1953.

15. Reed, Robert D.

Flight Measurements of Horizontal-Tail Loads on the Bell X-5 Research Airplane at a Sweep Angle of 58.7°. NACA RM H55E20a, 1955.

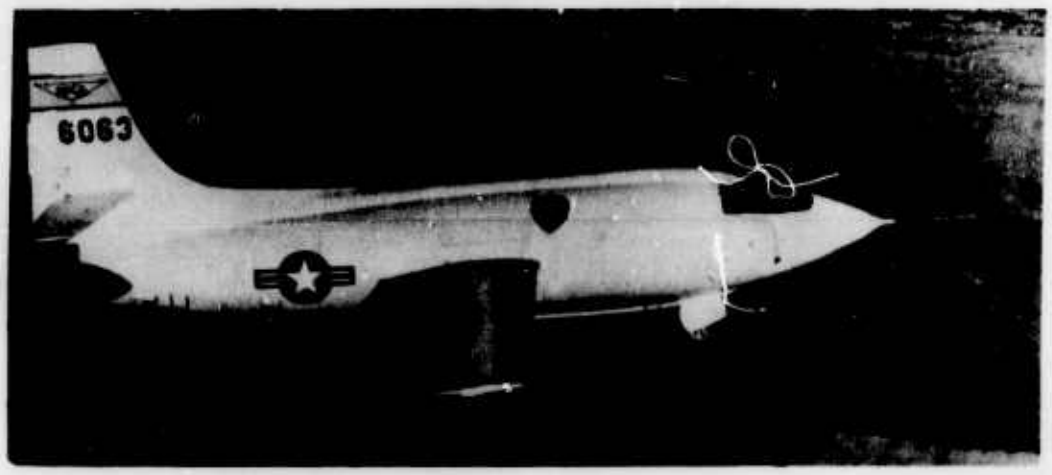

(a) X-1 airplane

(b) X-5 airplane

(c) XF-92A airplane

Fig.1 Photographs of the airplanes

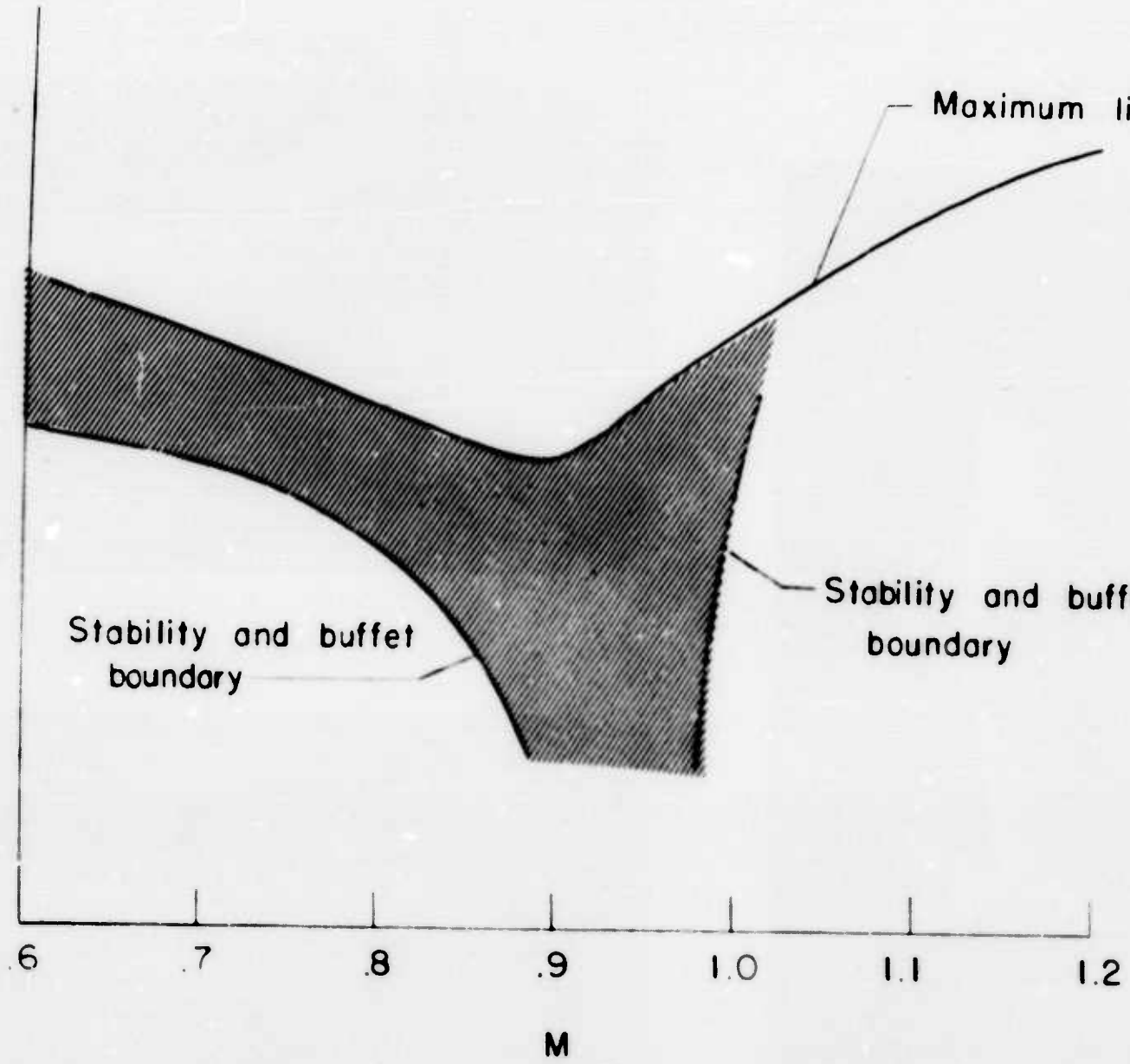

Fig.2 Sketch of flight regions

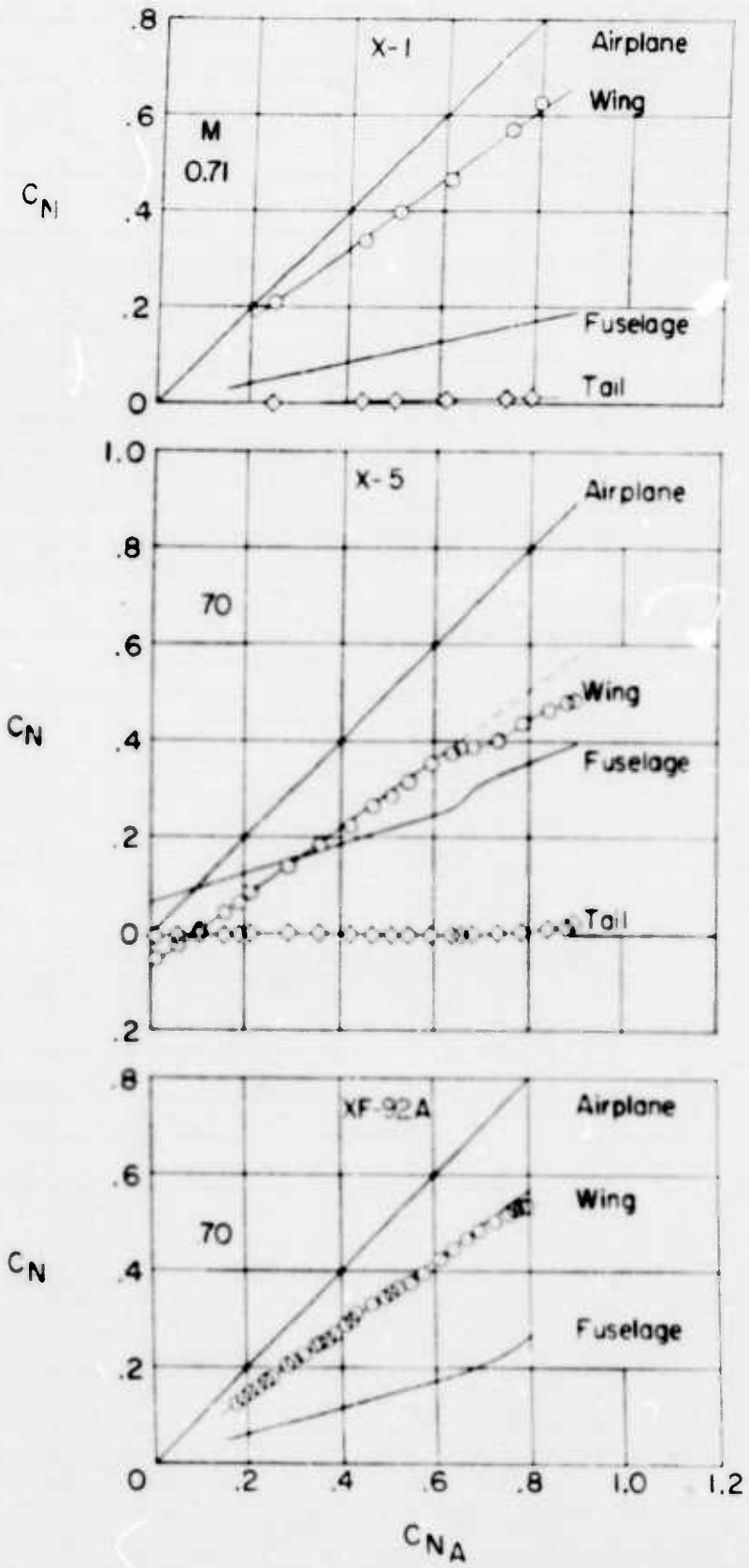

(a) M = 0.7

Fig.3 Division of airplane load

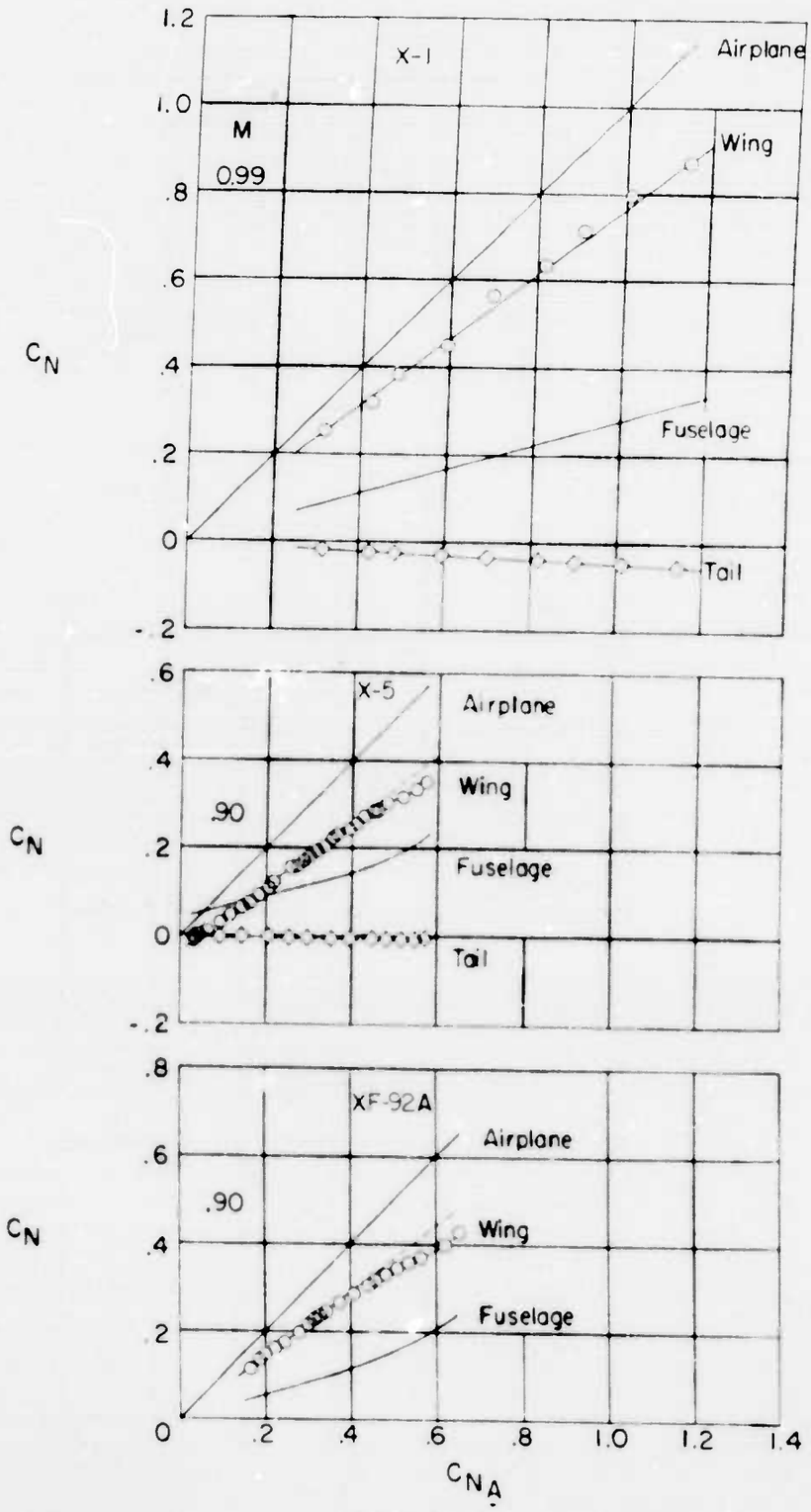

(b) $M \approx 0.9$

Fig. 3 (Concluded)

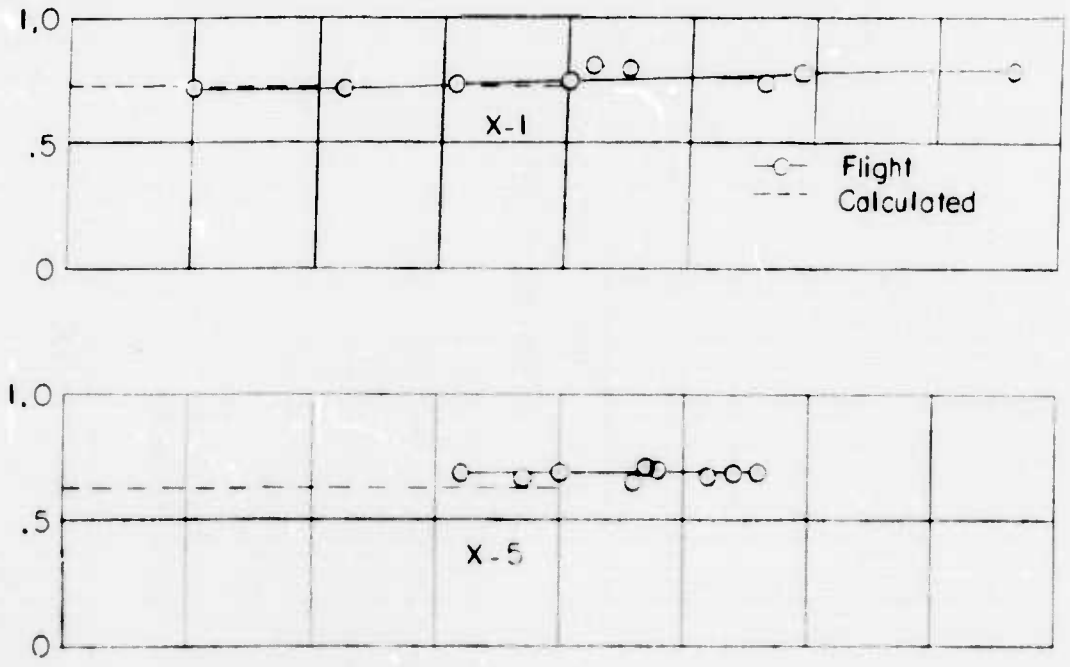

$\frac{dC_{N_w}}{dC_{N_{wf}}}$

Fig. 4 Mach number variation of the wing load to wing-fuselage load

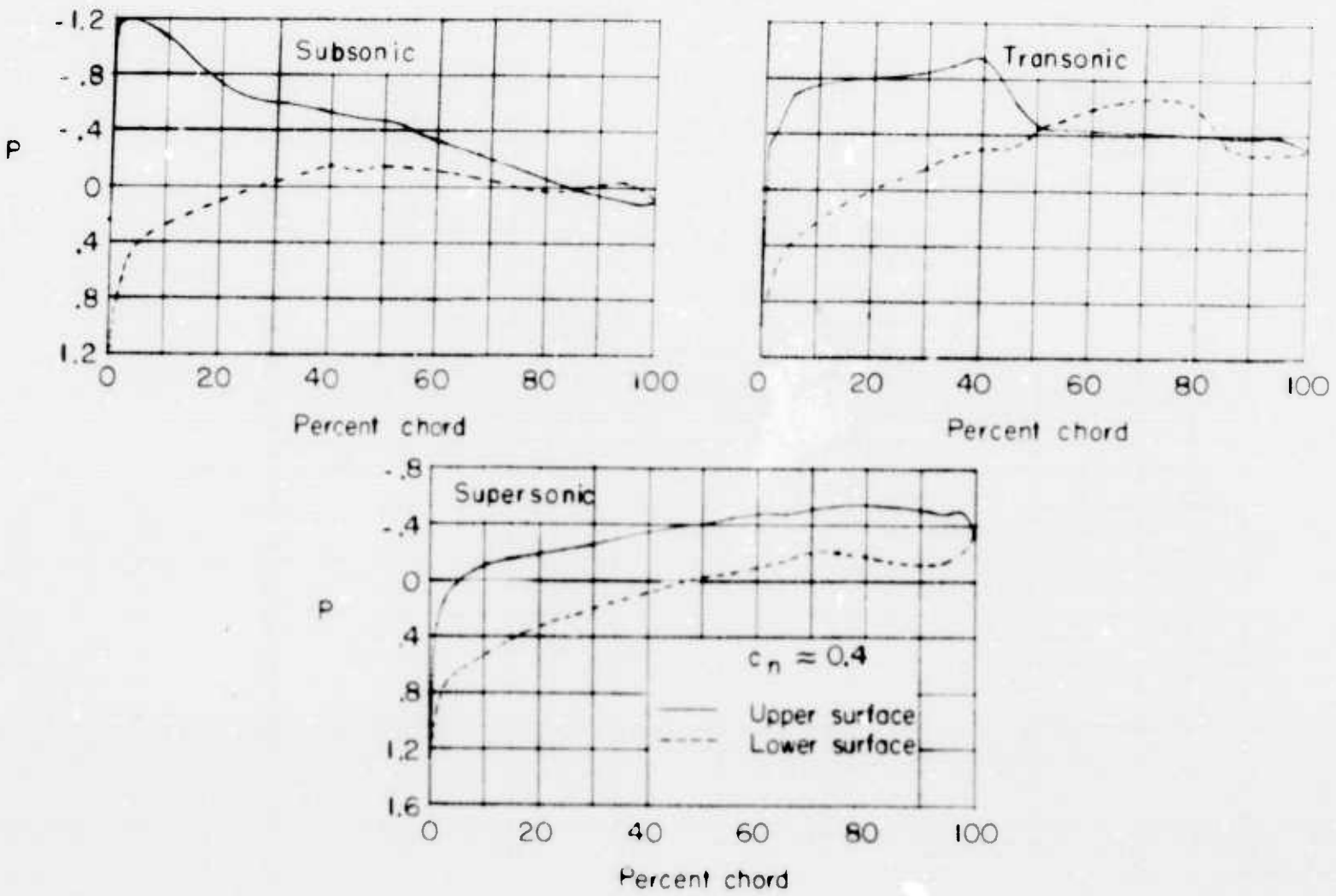

Fig.5 Chordwise pressure distribution of the X-1 wing at the panel semispan

Fig.6 Wing distribution of the section chordwise loading. $C_{N_w} \approx 0.40$

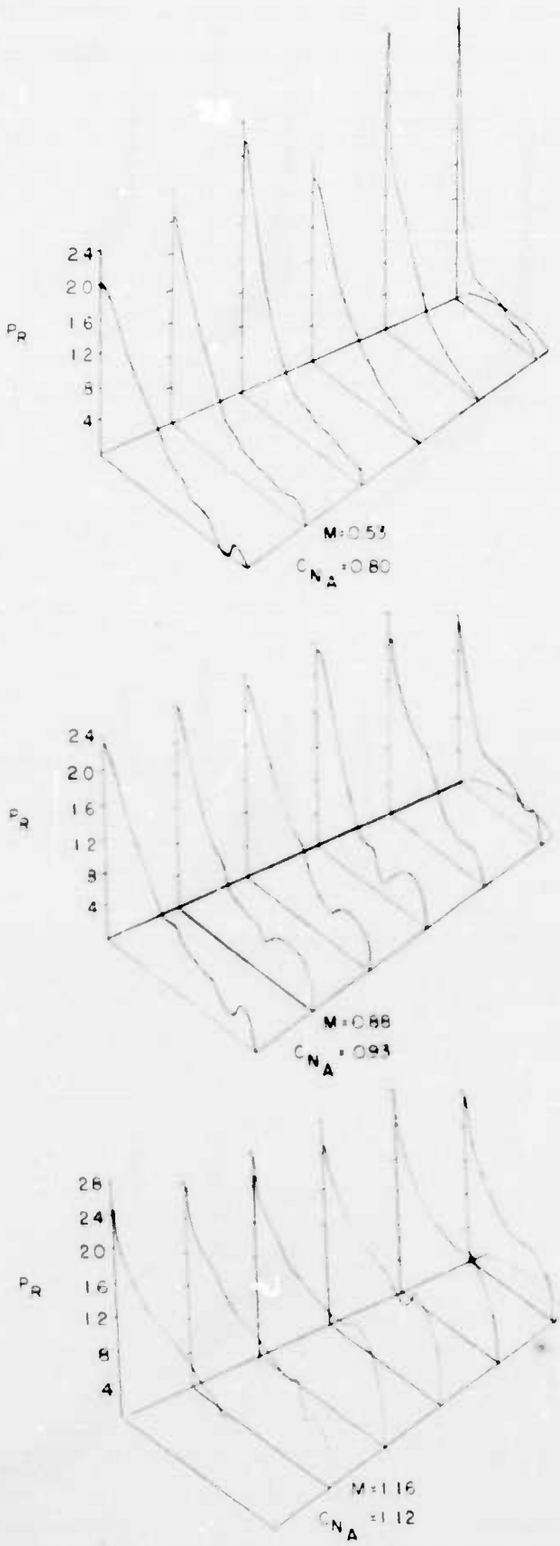

Fig. 7 Wing distribution of the section chordwise loading. High normal-force coefficient.

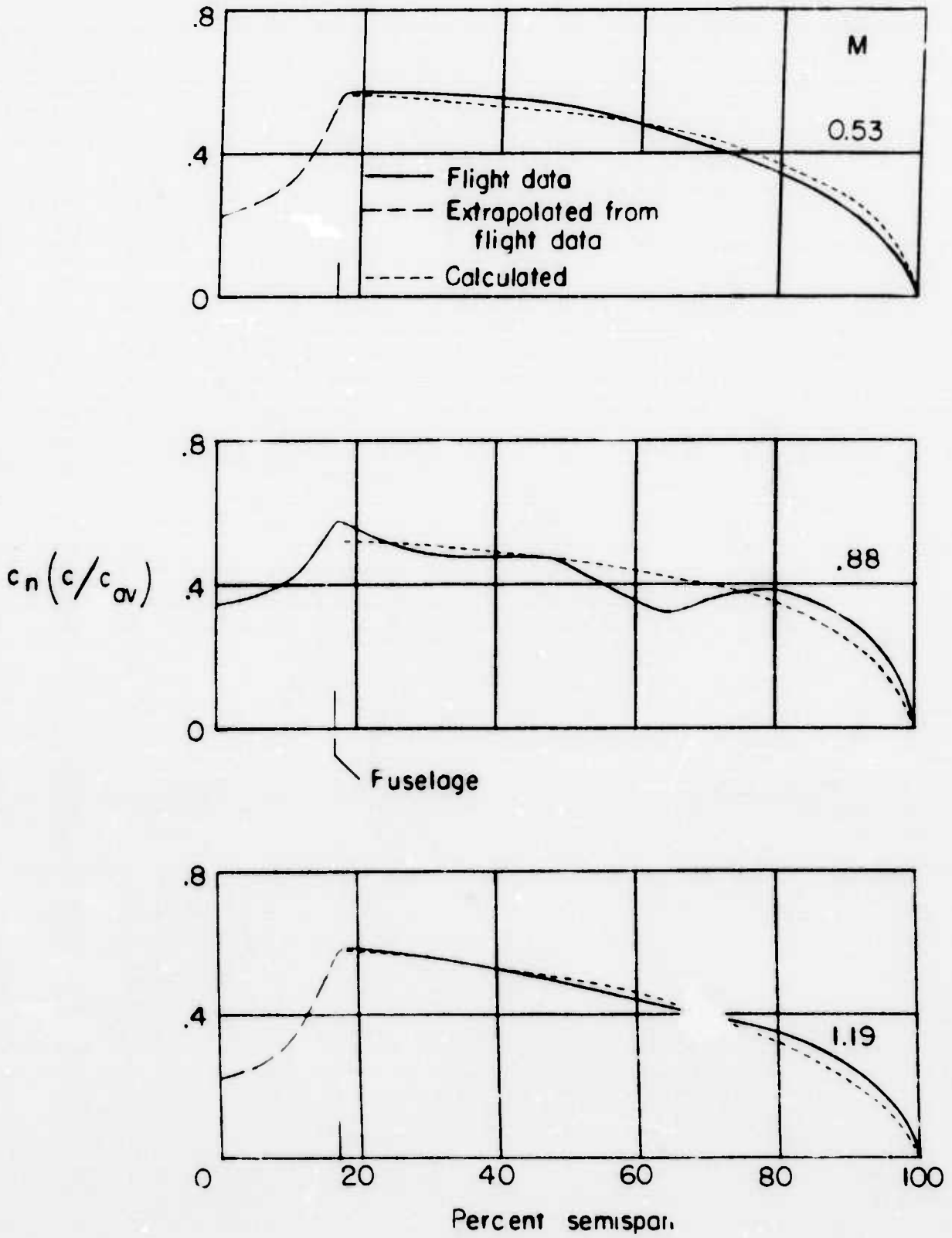

Fig. 8 Span load distribution. X-1 airplane

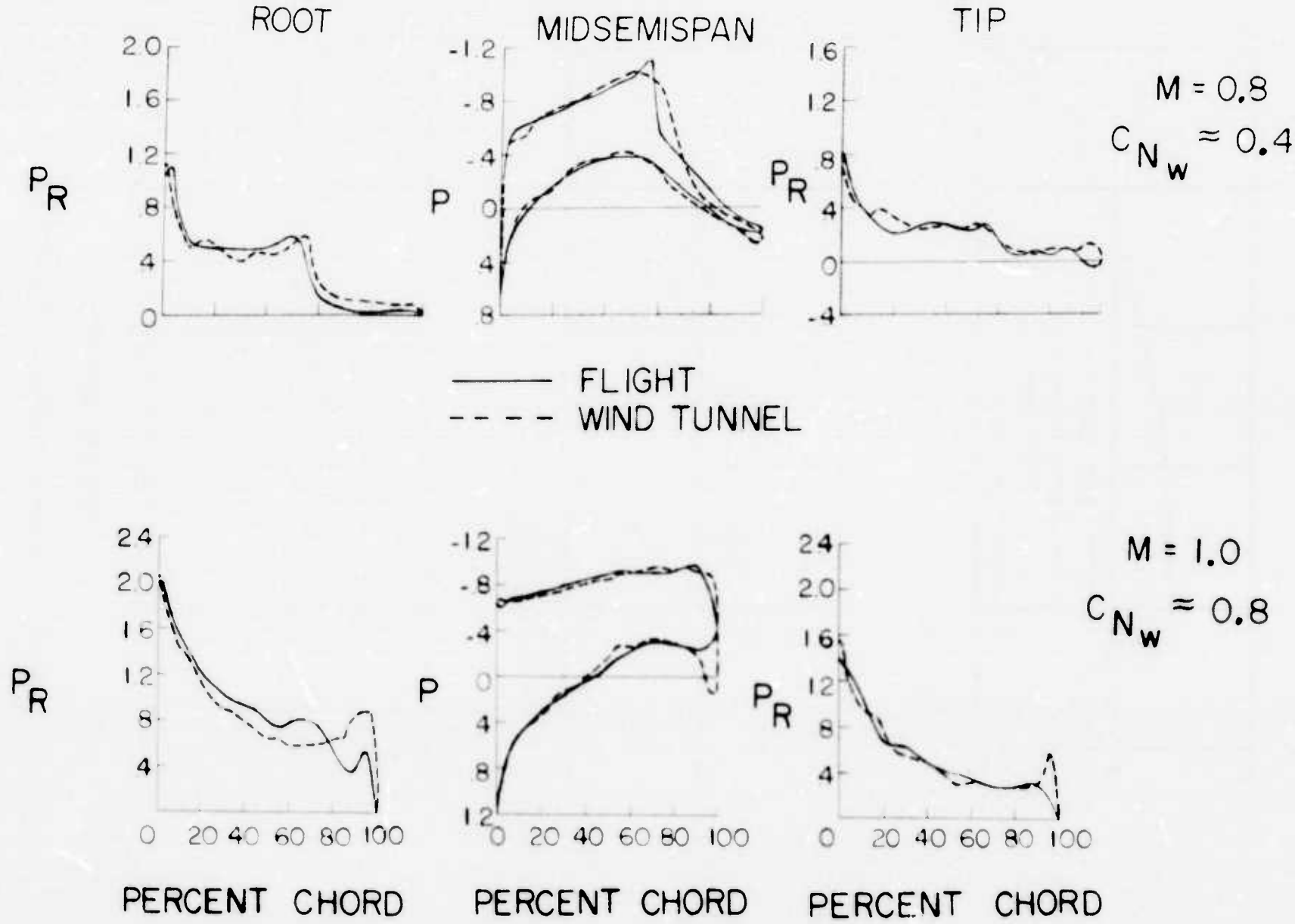

Fig.9 Comparison of flight and wind-tunnel section loading. X-1 airplane

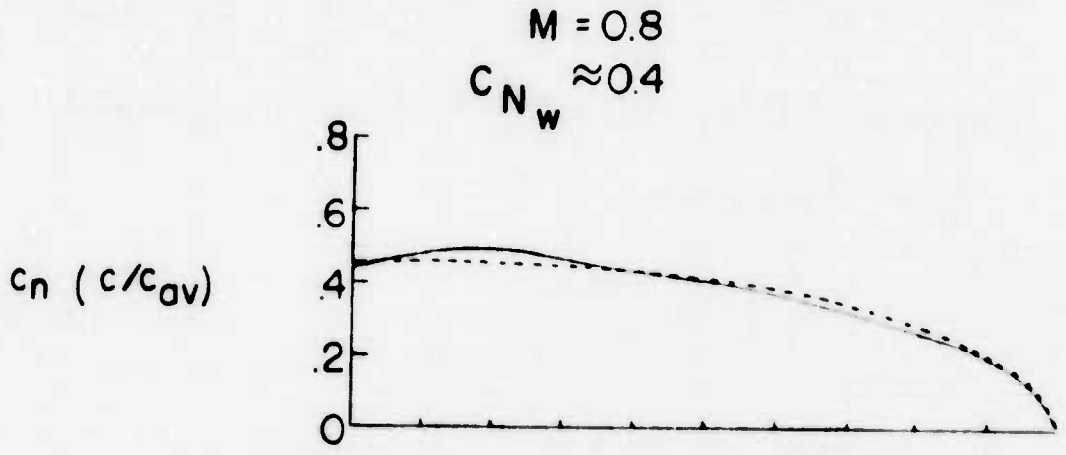

Fig. 10 Comparison of flight and wind-tunnel span loadings. X-1 airplane

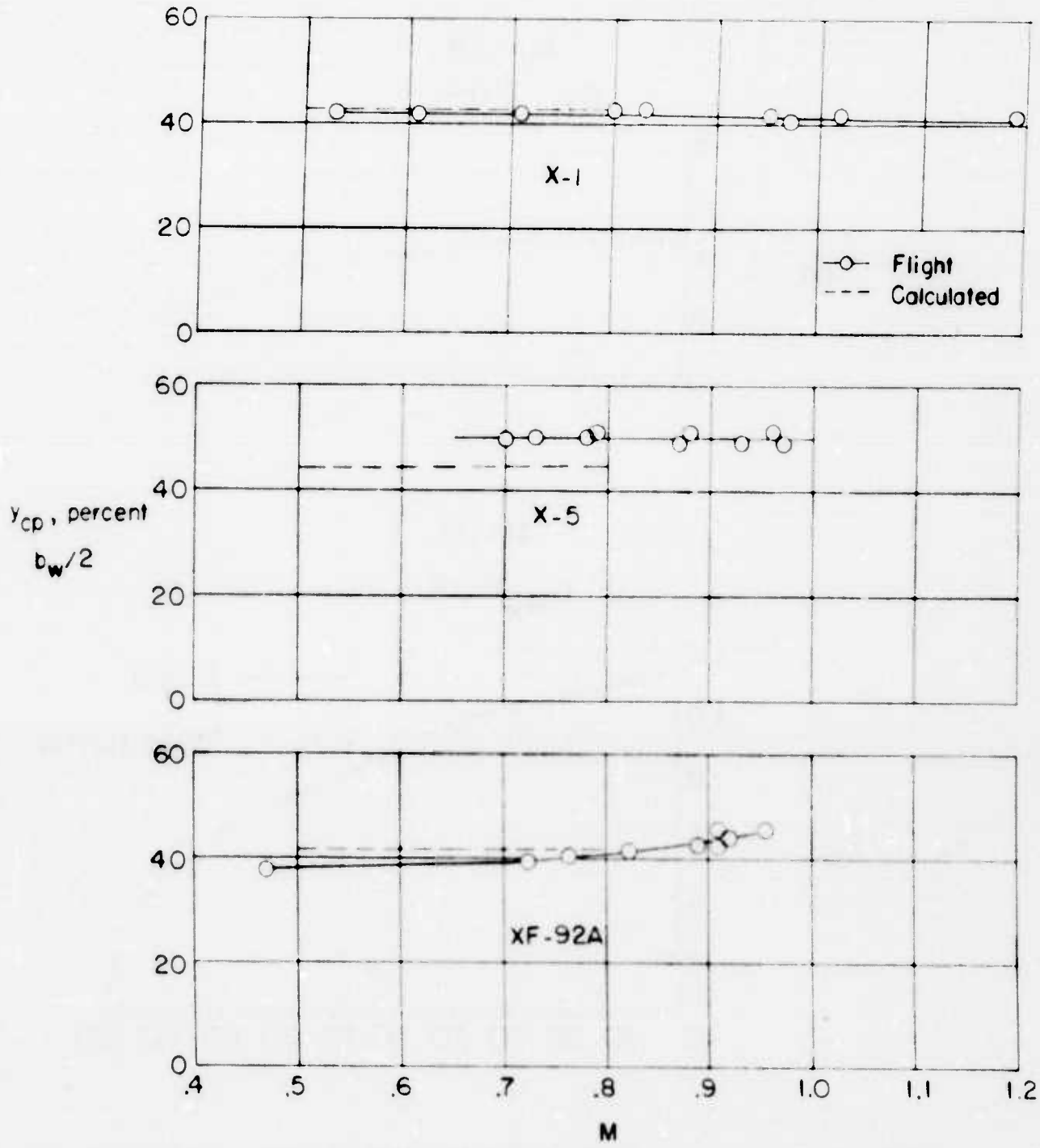

Fig. 11 Effect of Mach number on the wing lateral center of pressure

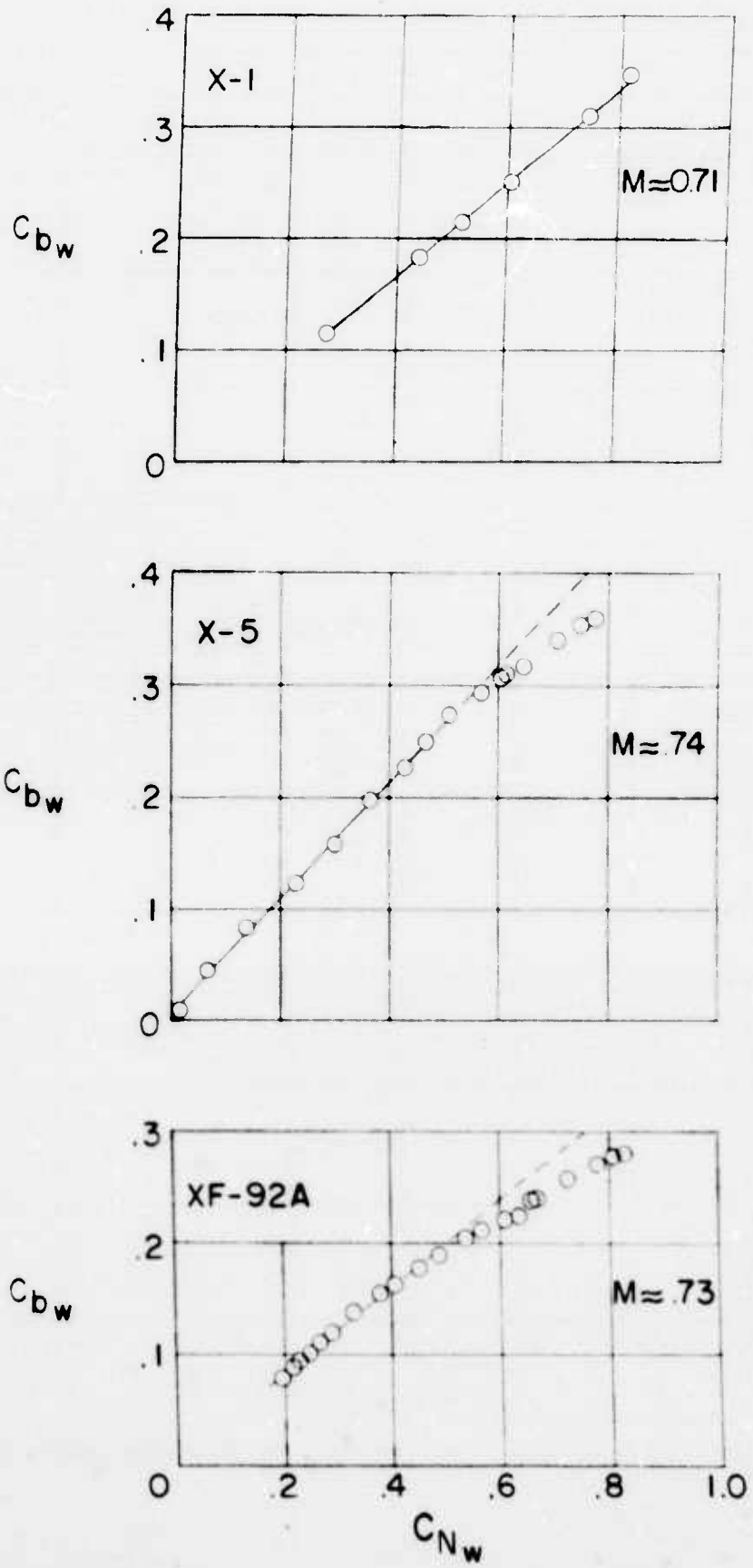

Fig. 12 Variation of wing bending-moment coefficient with wing normal load

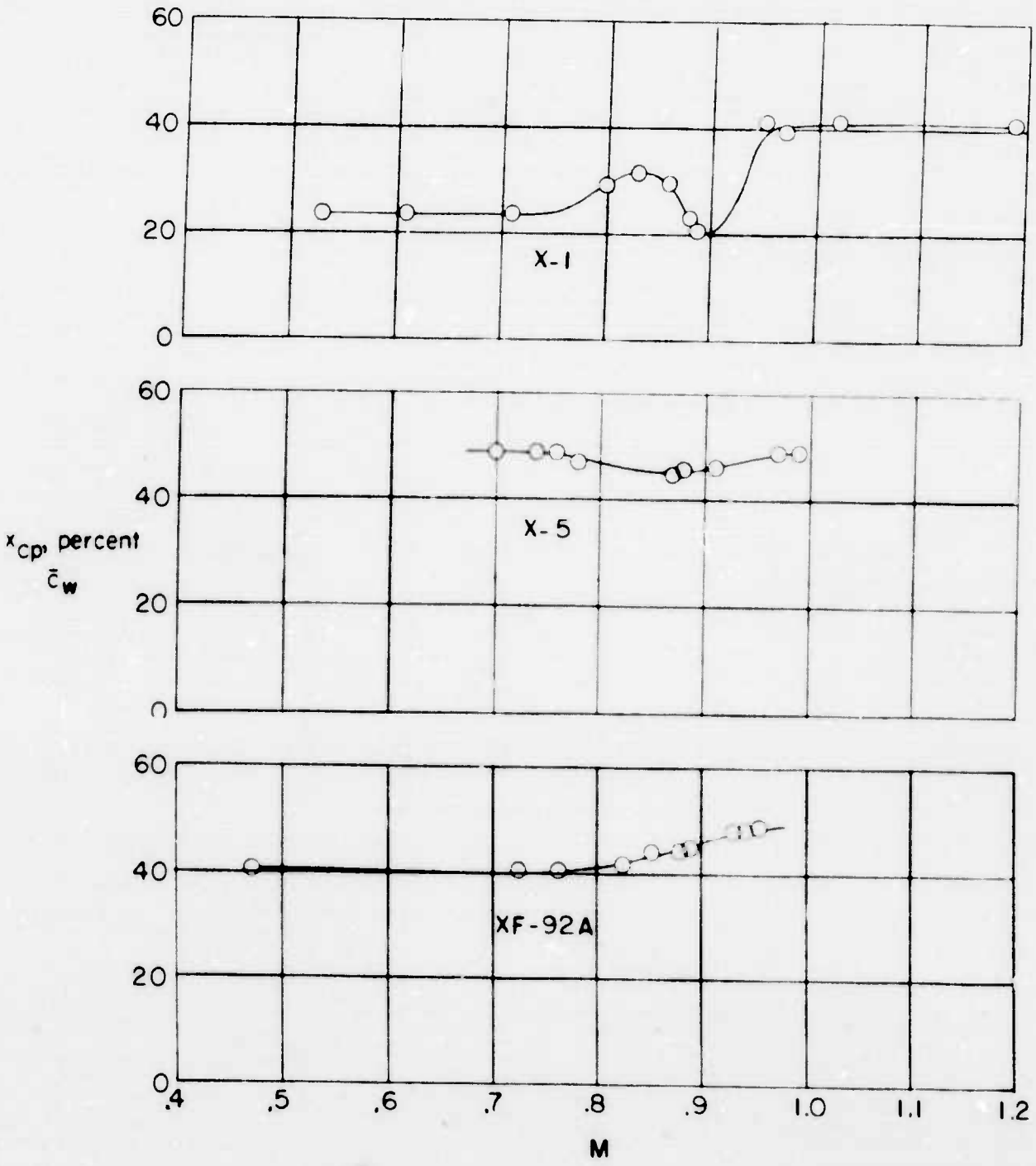

Fig.13 Effect of Mach number on the wing chordwise center of pressure

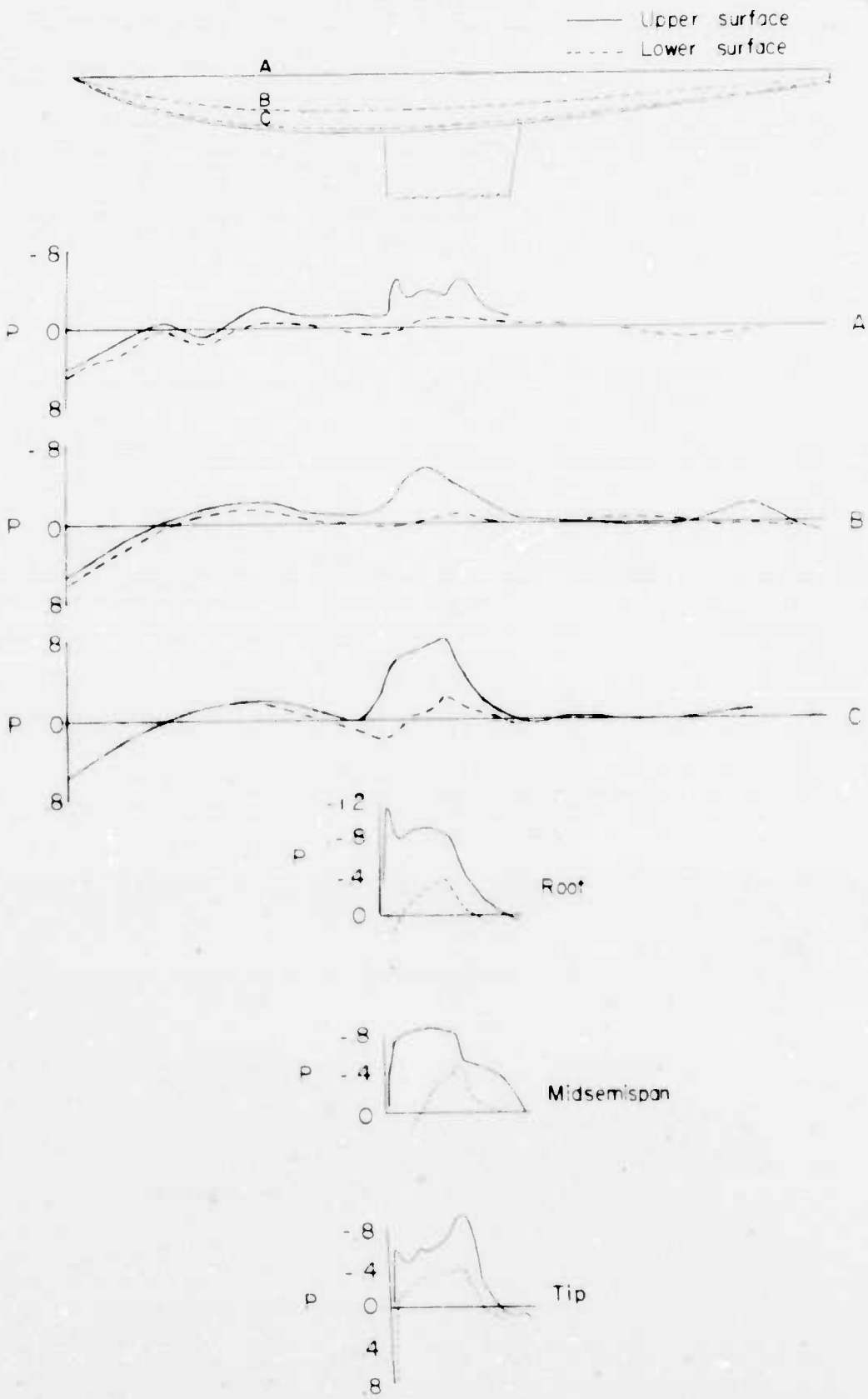

(a) $\alpha = 2^{o}$; M = 0.80

Fig. 14 Fuselage and wing pressure distribution of X-1 airplane

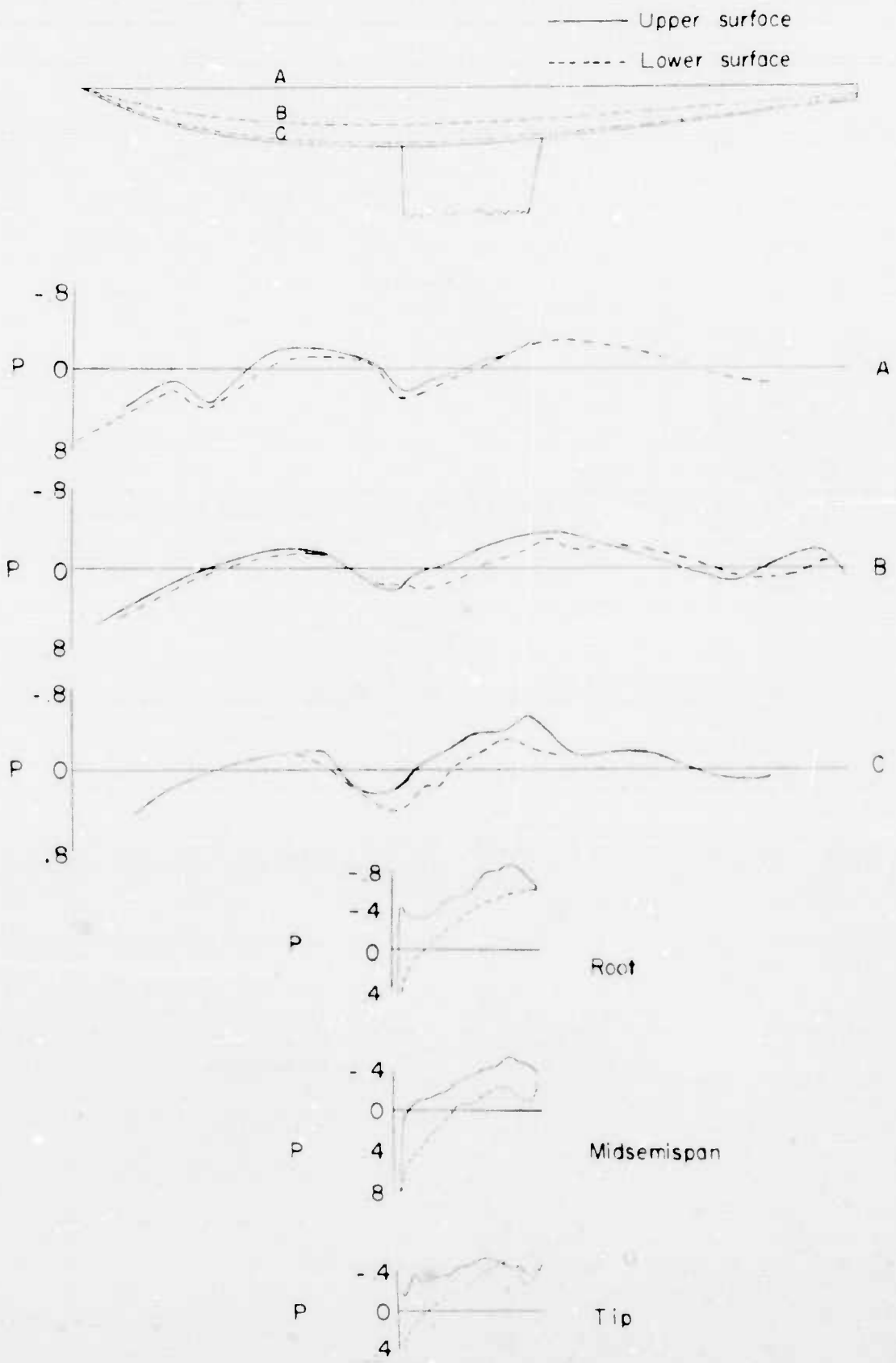

(b) $\alpha = 2^{o}$; M = 1.0

Fig.14 (Concluded)

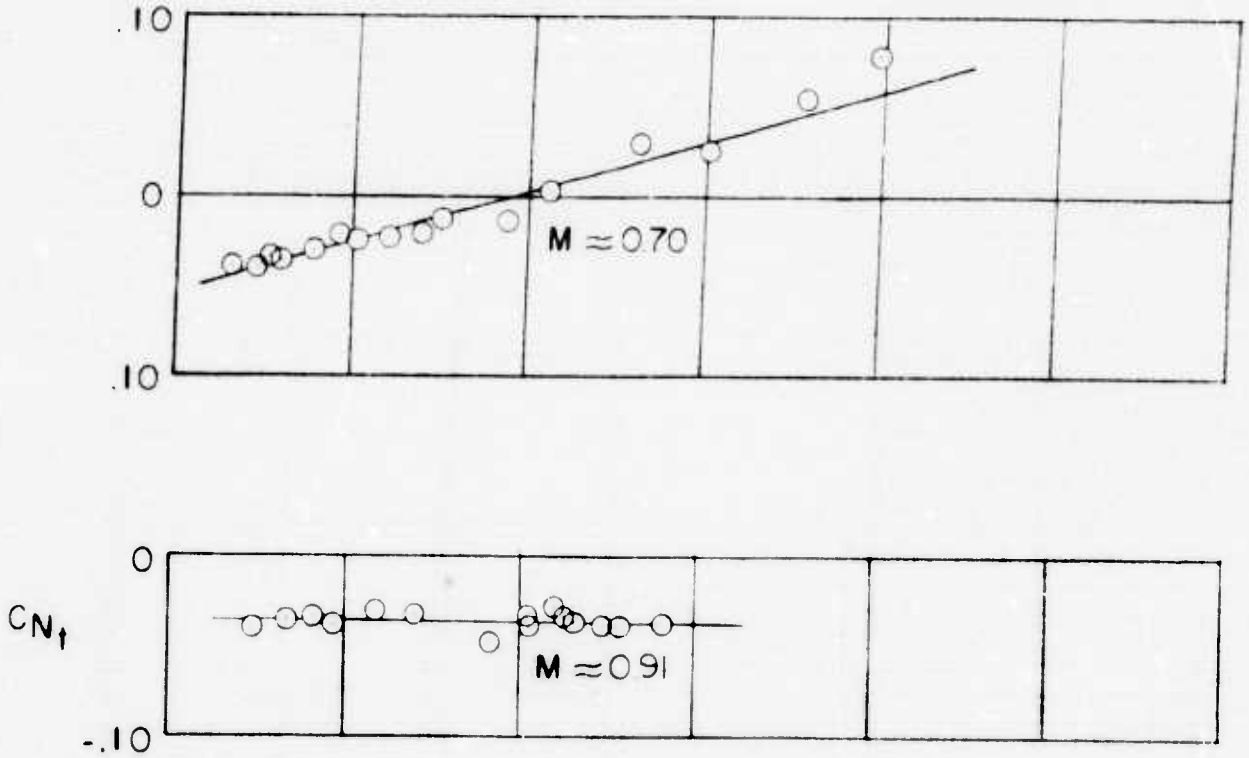

Fig. 15 Variation of horizontal tail normal load with airplane normal load. X-1 airplane

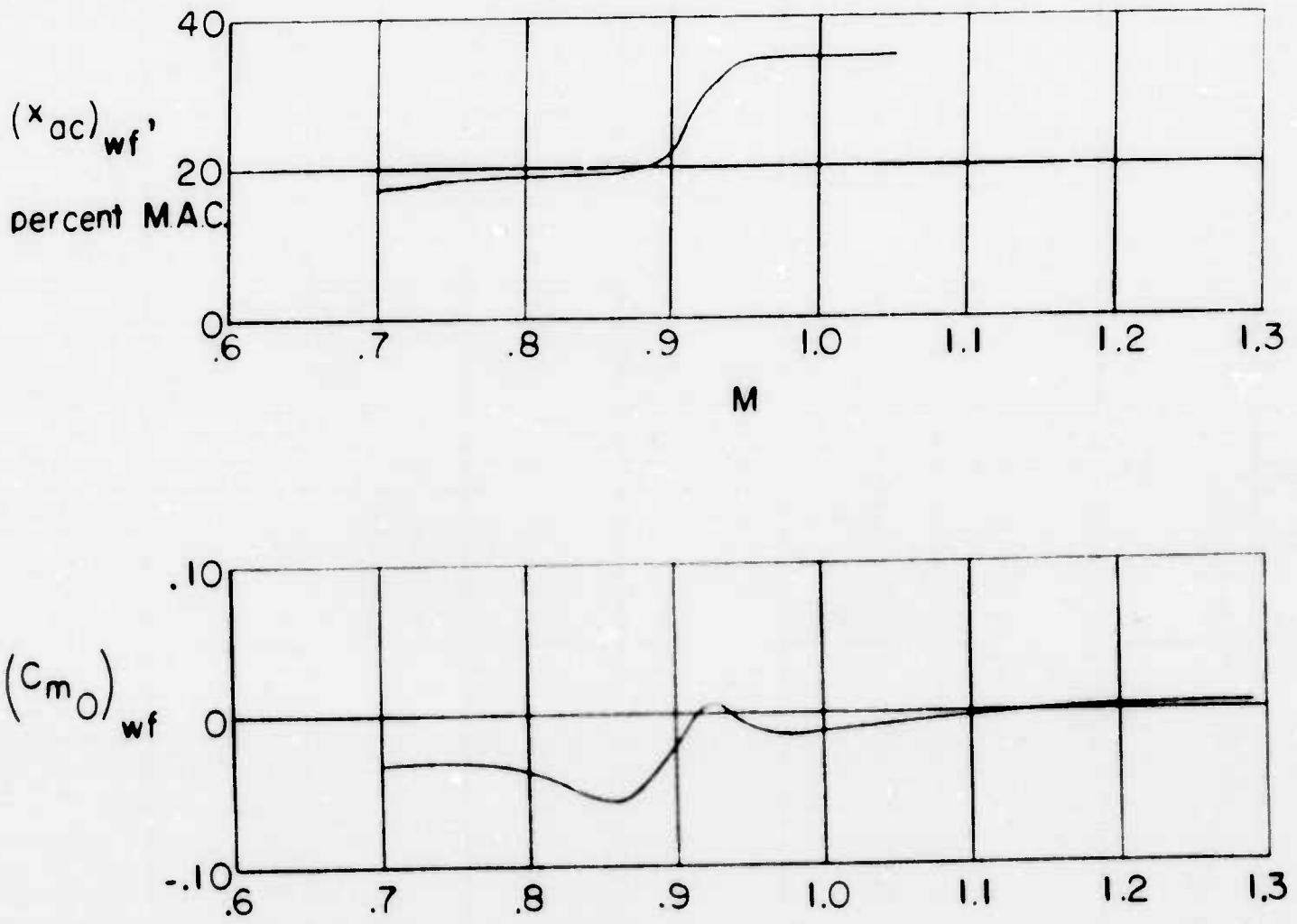

Fig. 16 Variation of wing-fuselage parameters with Mach number. X-1 airplane

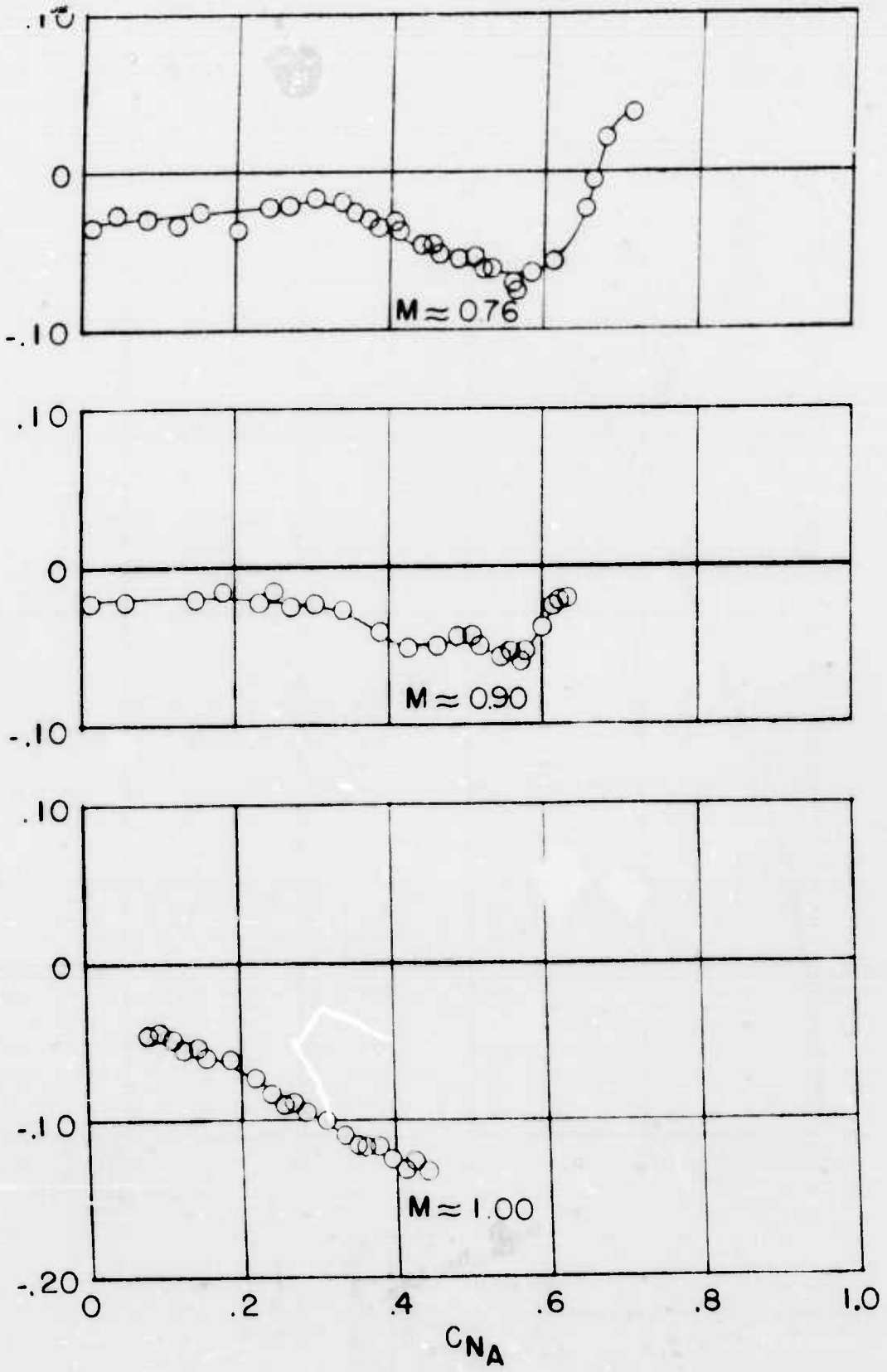

Fig. 17 Variation of the horizontal tail normal load with airplane normal load. X-5 airplane.

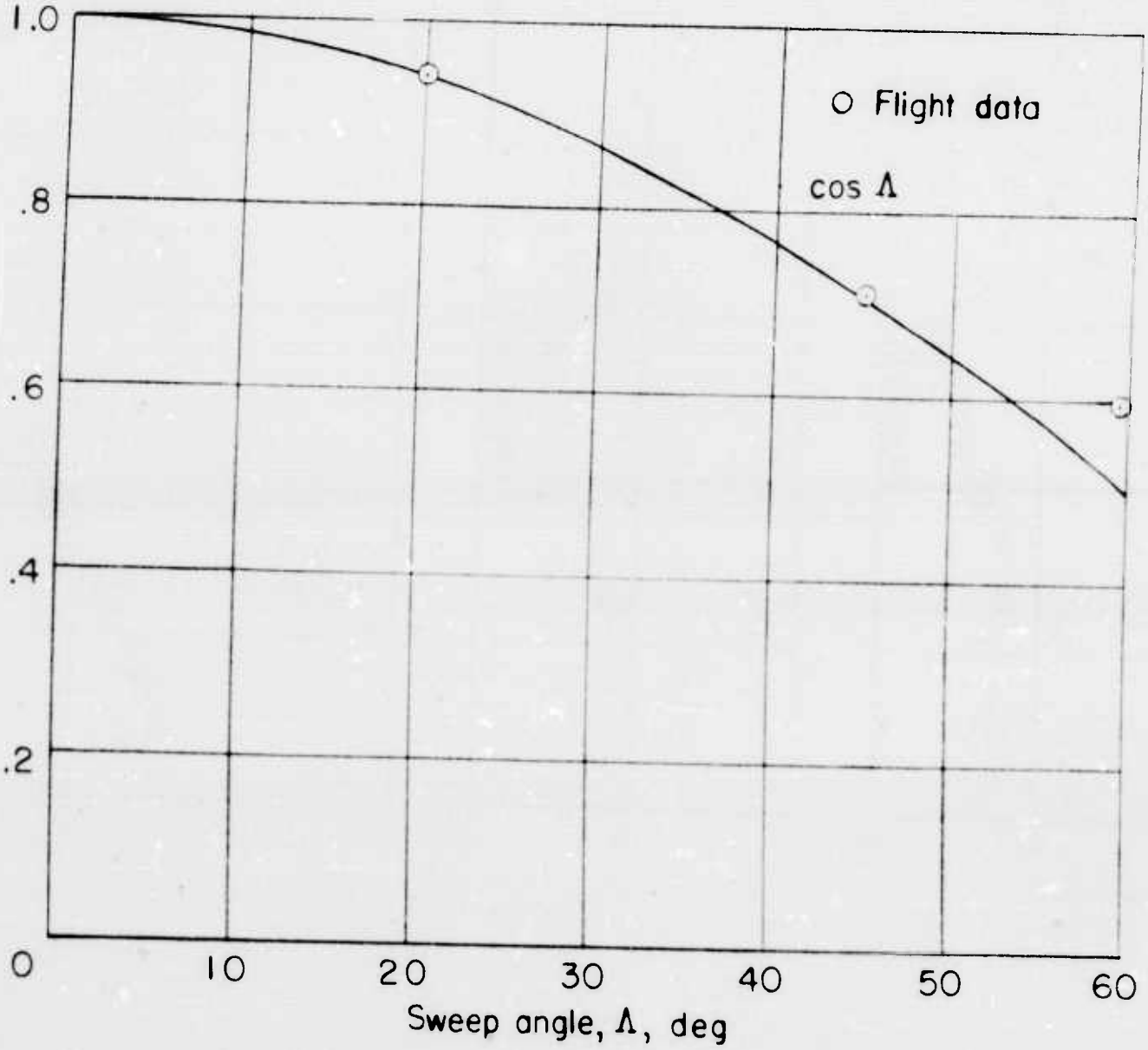

Fig. 18 Effect of sweep on gust response. X-5 airplane

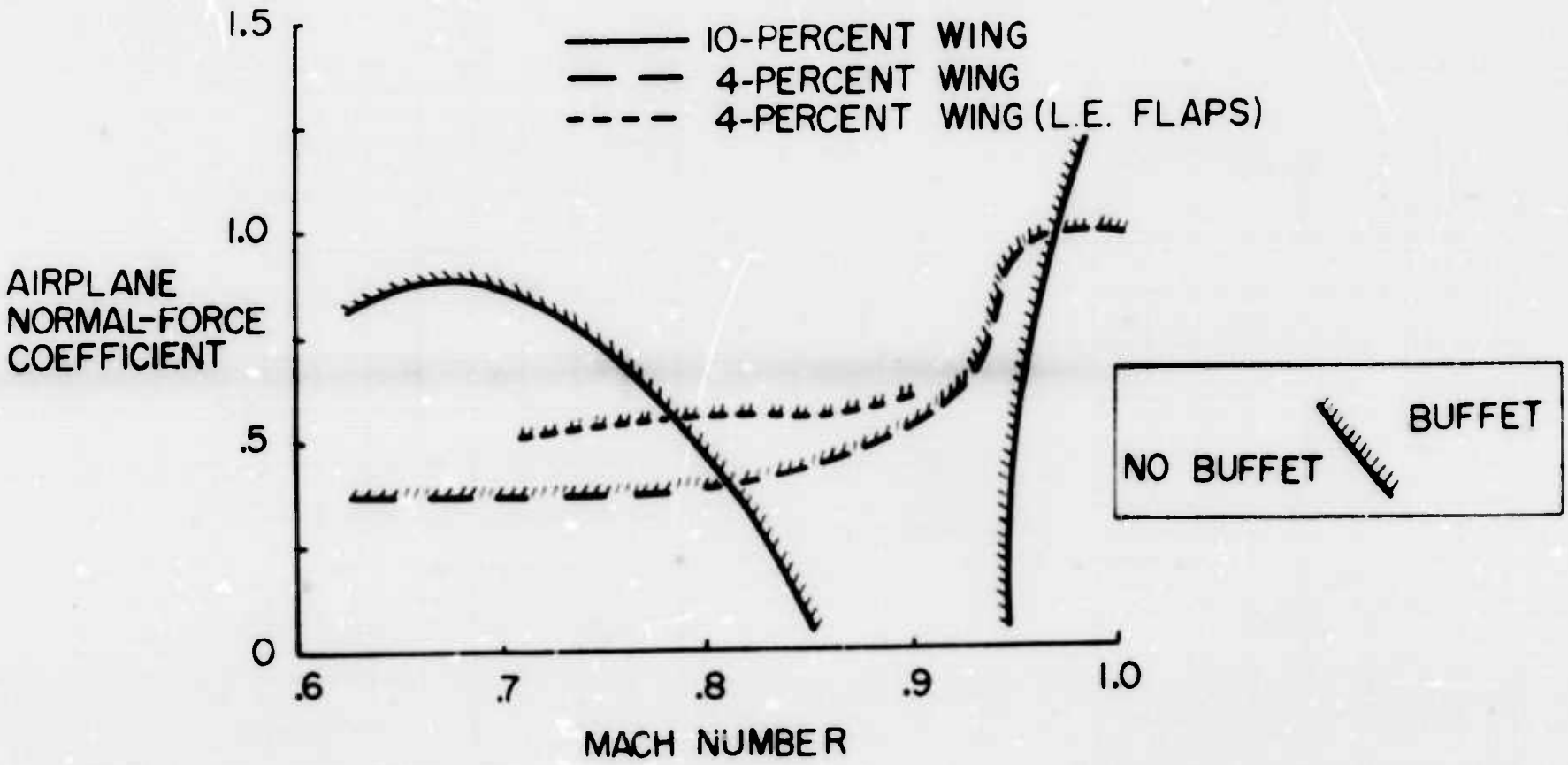

Fig.19 Effects of airfoil thickness on buffeting

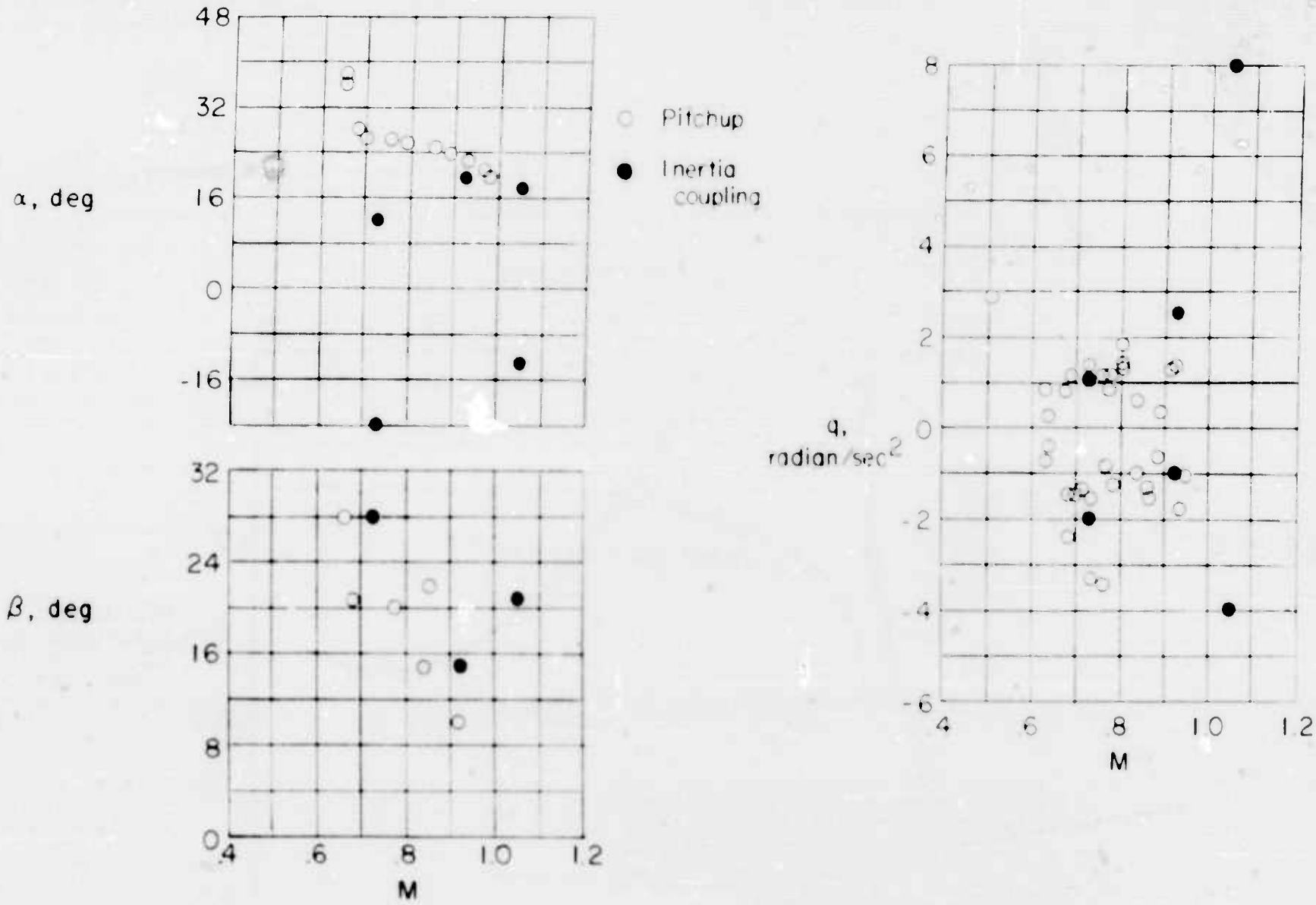

Fig.20 Flight conditions reached during uncontrolled maneuvers

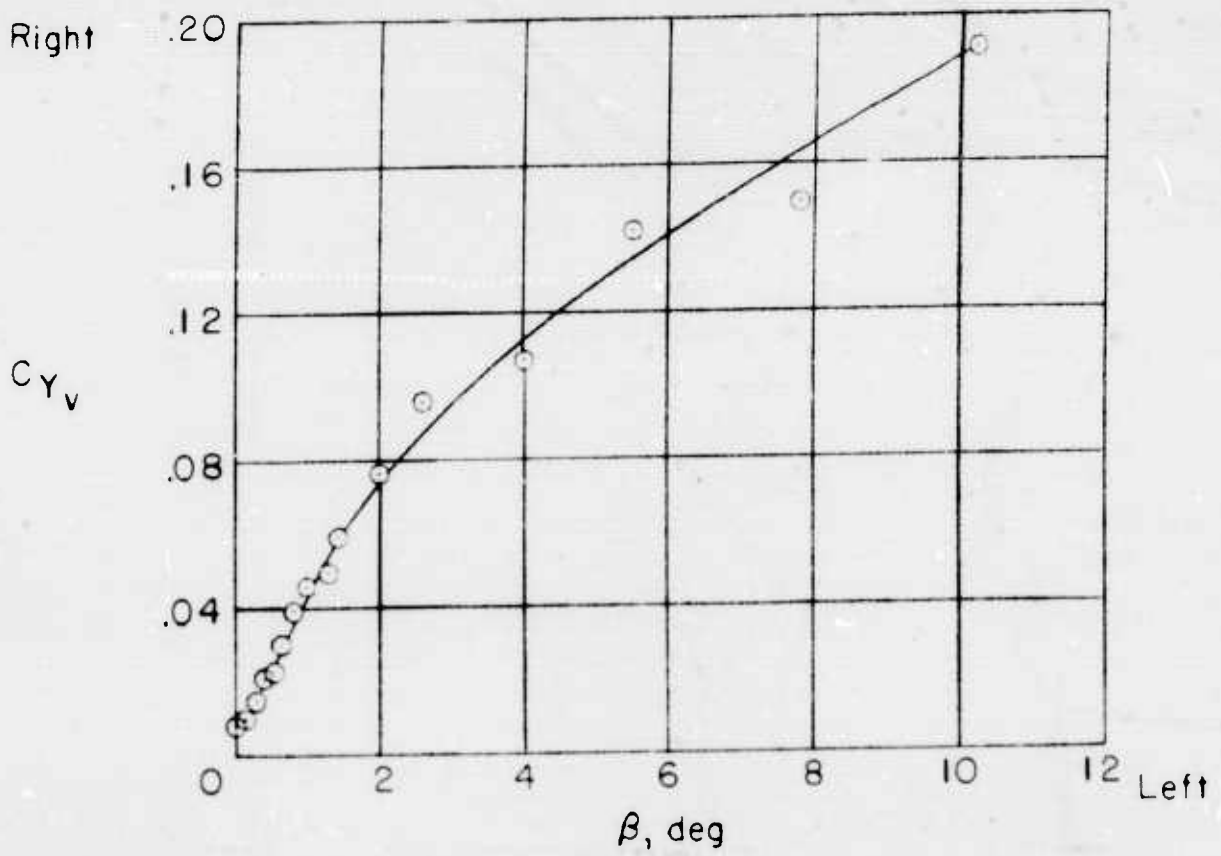

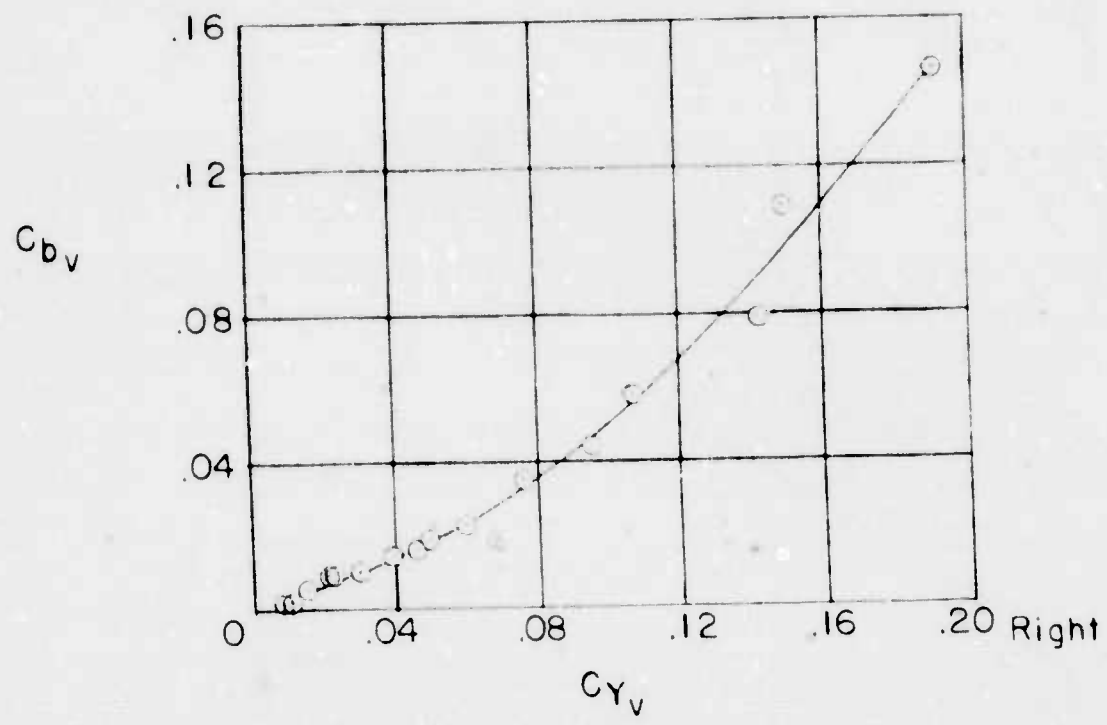

Fig.21 Effect of yaw on vertical tail loads at high angles of attack. X-5 airplane

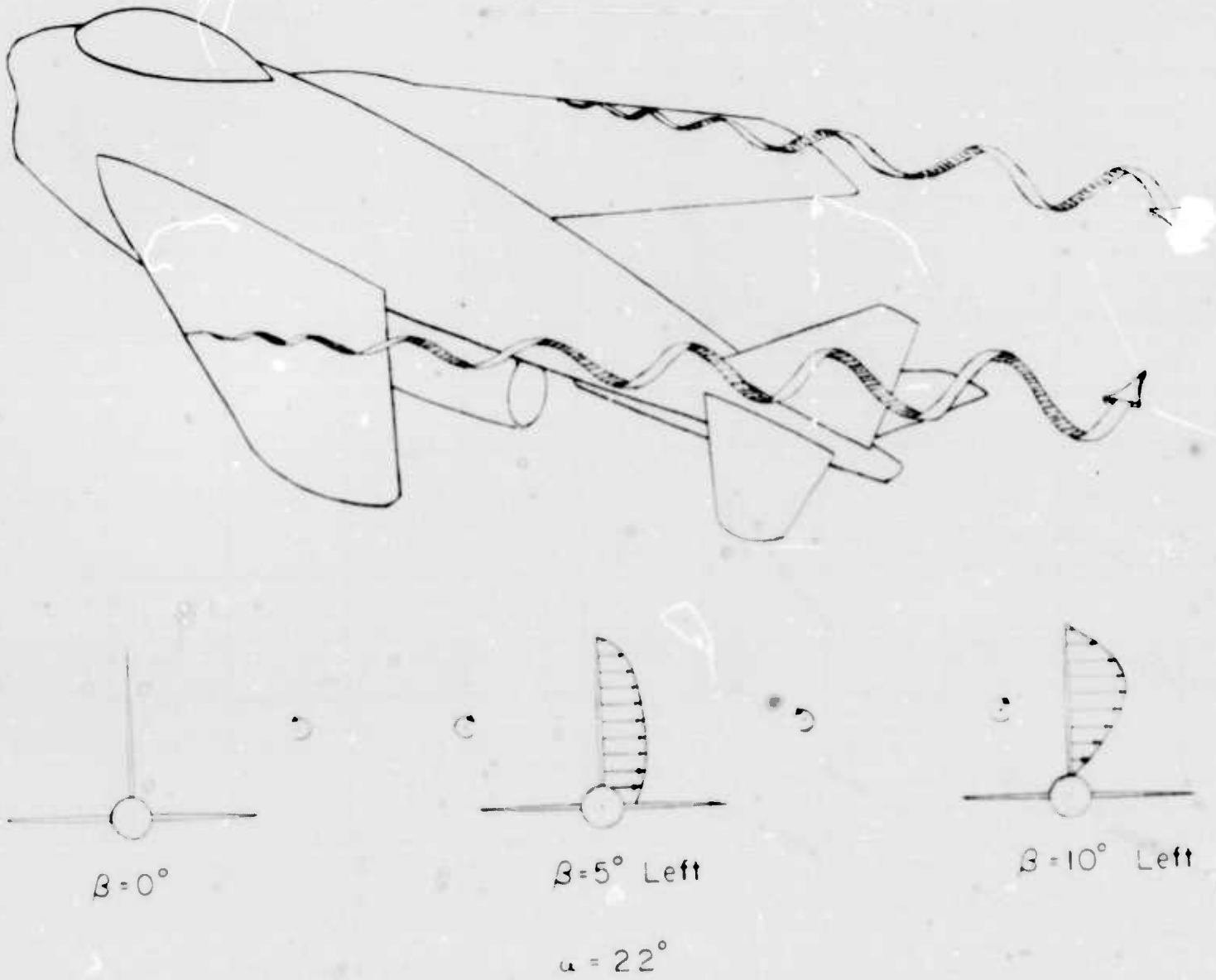

Fig.22 Vortex location from low-speed tunnel studies

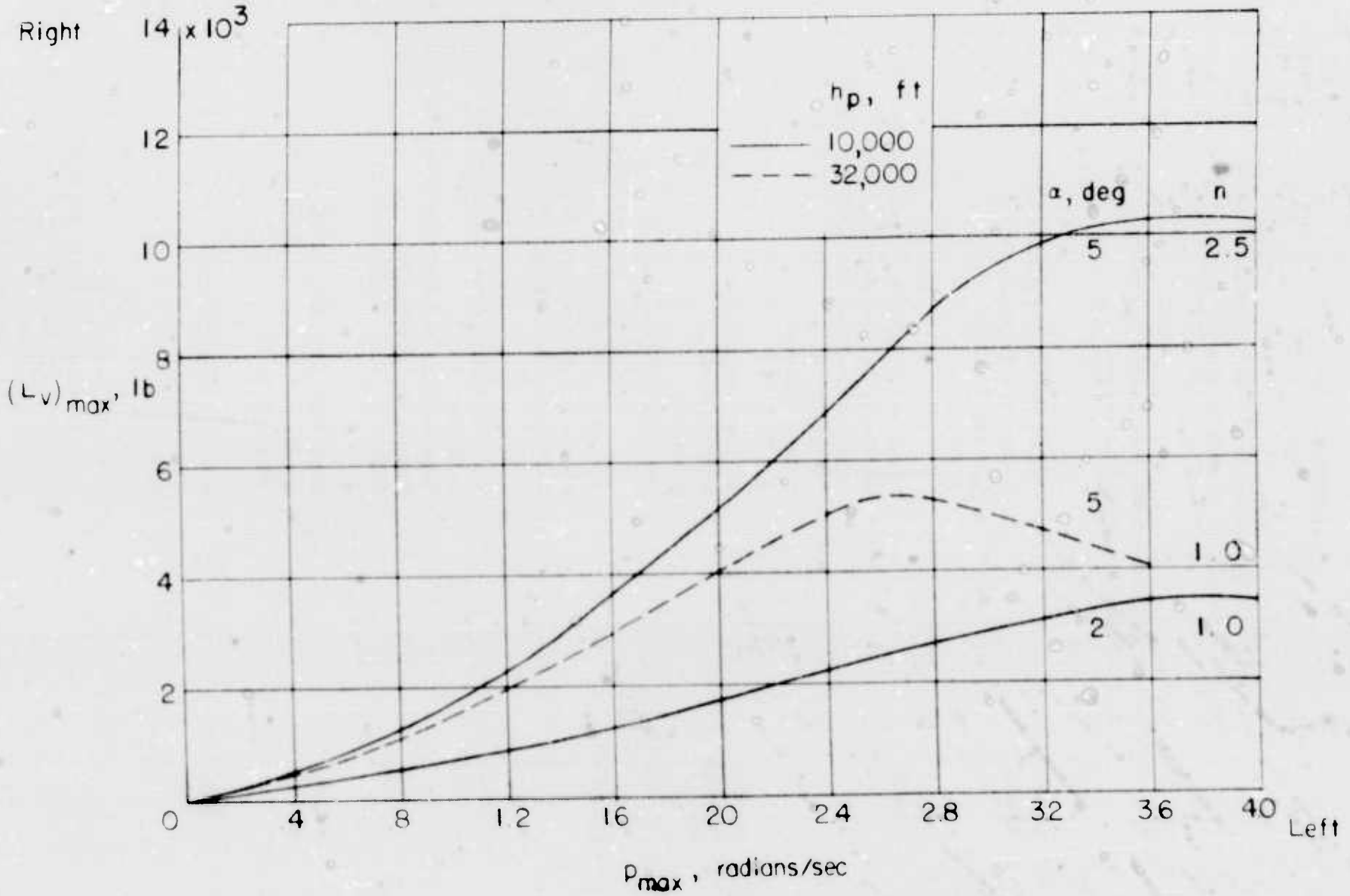

Fig. 23 Calculated vertical-tail loads during rolling maneuvers

DISTRIBUTION

Copies of AGARD publications may be obtained in the various countries at the addresses given below.

On peut se procurer des exemplaires des publications de l'AGARD aux adresses suivantes.

BELGIUM
BELGIQUE
Centre National d'Etudes et de Recherches Aéronautiques
11, rue d'Egmont
Bruxelles.

CANADA
Director of Scientific Information Services, Defence Research Board
Department of National Defence
'A' Building
Ottawa, Ontario.

DENMARK
DANEMARK
Military Research Board
Defence Staff
Kastellet
Copenhagen Ø.

FRANCE
O.N.E.R.A. (Direction)
25, avenue de la Division-Leclerc
Châtillon-sous-Bagneux (Seine)

GERMANY
ALLEMAGNE
Wissenschaftliche Gesellschaft für Luftfahrt
Zentralstelle der Luftfahrtdokumentation
Munchen 64, Flughafen
Attn: Dr. H.J. Rautenberg

GREECE
GRECE
Greek Nat. Def. Gen. Staff
B. MEO
Athens.

ICELAND
ISLANDE
Director of Aviation
C/o Flugrad
Reykjavik
Iceland

ITALY
ITALIE
Centro Consultivo Studi e Ricerche
Ministero Difesa - Aeronautica
Via Salaria 336
Rome.